NASA Contractor Report 166057

NASA-CR-166057
19830011116

NASA F-106B LIGHTNING TESTS

Billy D. Heady and Keith S. Zeisel

MCDONNELL DOUGLAS CORPORATION
McDonnell Aircraft Company
St. Louis, Missouri 63166

Contract NAS1-16202
January 1983

National Aeronautics and
Space Administration

Langley Research Center
Hampton, Virginia 23665

TABLE OF CONTENTS

This Page Intentionally Left Blank

LIST OF ILLUSTRATIONS

(cont'd)

(cont'd)

1.0 INTRODUCTION

This report summarizes the lightning simulation tests of the NASA F-106B research aircraft conducted between 29 March and 2 April 1982 at NASA Langley Research Center. This work was performed by the lightning laboratories (Department 256) of the McDonnell Aircraft Company (MCAIR).

The purpose of the test program was to measure the response of the aircraft's electromagnetic sensors and interior wire circuits to a controlled ground test environment that simulates the electromagnetic effects of a lightning strike. Specific objectives were to (1) compare the F-106 sensor responses with those of externally-mounted MCAIR sensors, (2) determine the variation of the sensor responses for controlled input waveform changes, (3) identify the characteristic aircraft resonances, and (4) measure the interior wire responses for different test conditions. The ultimate goal of the project is to compare the ground test data to actual flight test data obtained from lightning strikes in active thunderstorms. The comparison of these two sources of data will provide valuable information needed to assess the fidelity of lightning simulation ground test techniques.

Two completely different types of test configurations and aircraft stimuli were used to accomplish the test objectives. For most of the testing the aircraft was pulsed directly using a Marx generator connected to the aircraft's pitot tube and a coaxial current return system. However, one day of testing was conducted using a parallel wire transmission line to radiate the aircraft so that its natural resonant frequencies would be excited without any external connections.

2.0 F-106B BACKGROUND AND DESCRIPTION

NASA's Langley Research Center is currently conducting a thunderstorm hazards research program using the specially-instrumented F-106B aircraft. One of the program tasks is to measure the aircraft's response to direct lightning strikes. The intent of the research is to refine the characterization of the lightning environment. The research is motivated by the need to gather more information on lightning/aircraft interaction processes so that the protection designs of future aircraft systems might be optimized. During the 1980 and 1981 flight programs, 20 strikes were received in 180 thunderstorm penetrations.[1] The ground tests, discussed in this report, were conducted prior to the start of the 1982 flight program.

The F-106B aircraft contains a set of ten specially-designed electromagnetic sensors[2] and two interior wire circuits which can be monitored in flight by either expanded-memory digital or wide-band analog data channels. Figure 1 shows the approximate sensor locations. The I and $\dot{I}$ sensors are located at the base of the nose boom. Flat plate $\dot{D}$ sensors are located on the lower forward fuselage, on the left side of the vertical fin, and under each wing near the wing tip. Semi-circular loop $\dot{B}$ sensors are located on either side of the aft upper fuselage and under the wings near the outside of the main landing gear doors. The $\dot{B}$ sensor on the right side of the fuselage is oriented to measure longitudinal current down the axis of the aircraft. The other three $\dot{B}$ sensors are oriented to measure transverse current flow.

The two interior wire circuits are each unshielded single wires that are shorted to the airframe at one end and monitored across 50 ohms for their induced voltage response at the other end. One wire is shorted to the airframe near the left wing tip and runs in the leading edge of the wing to the

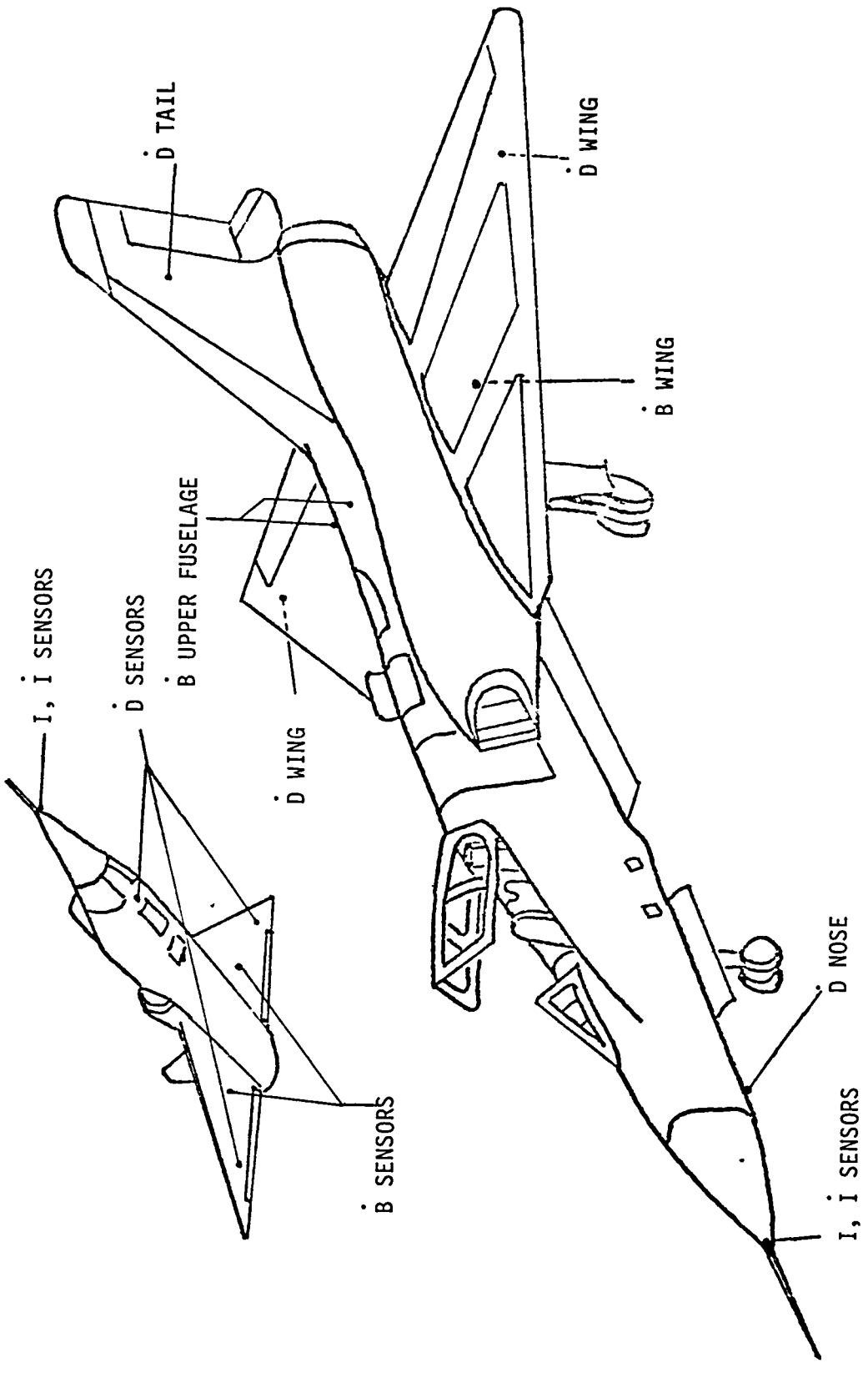

FIGURE 1 - NASA F-106B SENSOR LOCATIONS

FIGURE 1

instrumentation system. The other wire is shorted to the nose bulkhead and runs through the lower fuselage to the instrumentation system.

The instrumentation system is located in a shielded enclosure in the missile bay. The system includes digital and analog transient recorders and the instrumentation recorder for permanent data storage. The system power is isolated from the main aircraft power by a motor-generator set with a non-conducting coupler. Shielded coaxial cables transfer the passive electromagnetic sensor outputs to the instrumentation system.

3.0 TEST CONFIGURATIONS

Both direct attachment and radiated field tests were performed on the F-106B. The direct attachment tests were performed using a typical lightning simulation test configuration with the aircraft being the inner conductor of a "coaxial" transmission line that was pulsed by a Marx generator. Generator output voltages of 240 kV, and current levels of 2.6, 1.6, and 1.0 kA were used in this testing. The radiated tests were performed with the aircraft located within a large, terminated two-wire transmission line system. In these tests the free-standing aircraft was radiated with an electric field vector parallel to its axis when the Marx generator was fired into the long, two-wire transmission line. This section briefly describes each of these two test configurations. Appendix A describes more fully the major MCAIR test equipment used in both configurations.

3.1 DIRECT ATTACHMENT TEST SETUP. For the direct attachment tests, the aircraft placement and test setup was similar to that used previously by NASA in the F-106B lightning safety tests.[3] The principal test configuration differences in these tests and those conducted previously were: (1) the aircraft was isolated from ground potential using high-voltage dielectric pads beneath each landing gear wheel, (2) a high-voltage Marx generator was used to produce the system stimulus instead of a high-current capacitor system, (3) during some tests, a spark gap was incorporated in the output line from the aircraft to the return conductors, and (4) the aircraft sensors, interior wires, and external MCAIR sensors were monitored using fiber optic data links.

Figure 2 is an overall schematic of the test setup, and Figure 3 is a photograph showing the aircraft placement. The aircraft was first towed onto partially-assembled isolation pads. Then the pads were completed (see Figure 4),

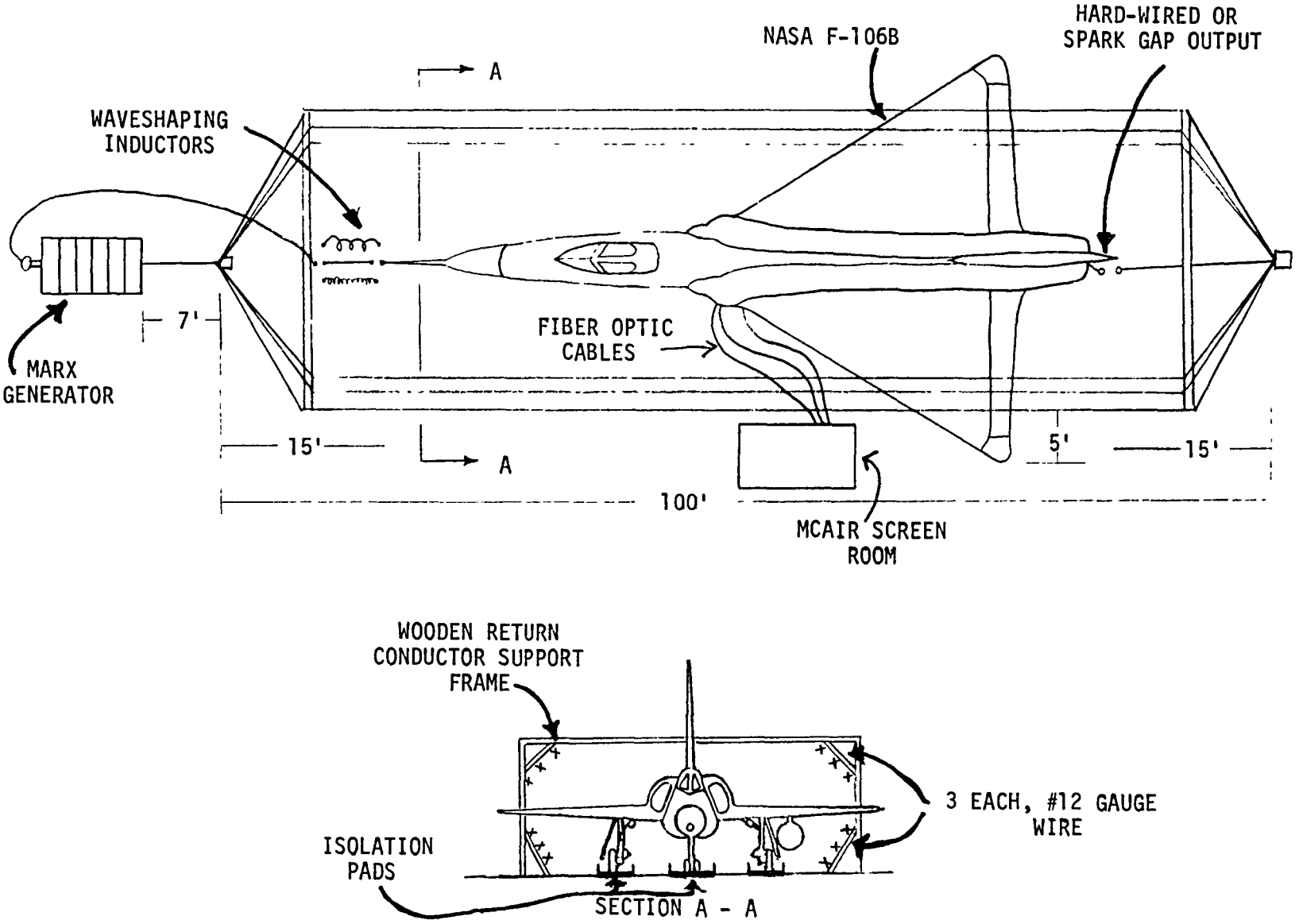

FIGURE 2 - SCHEMATIC OF DIRECT TEST SETUP

FIGURE 2

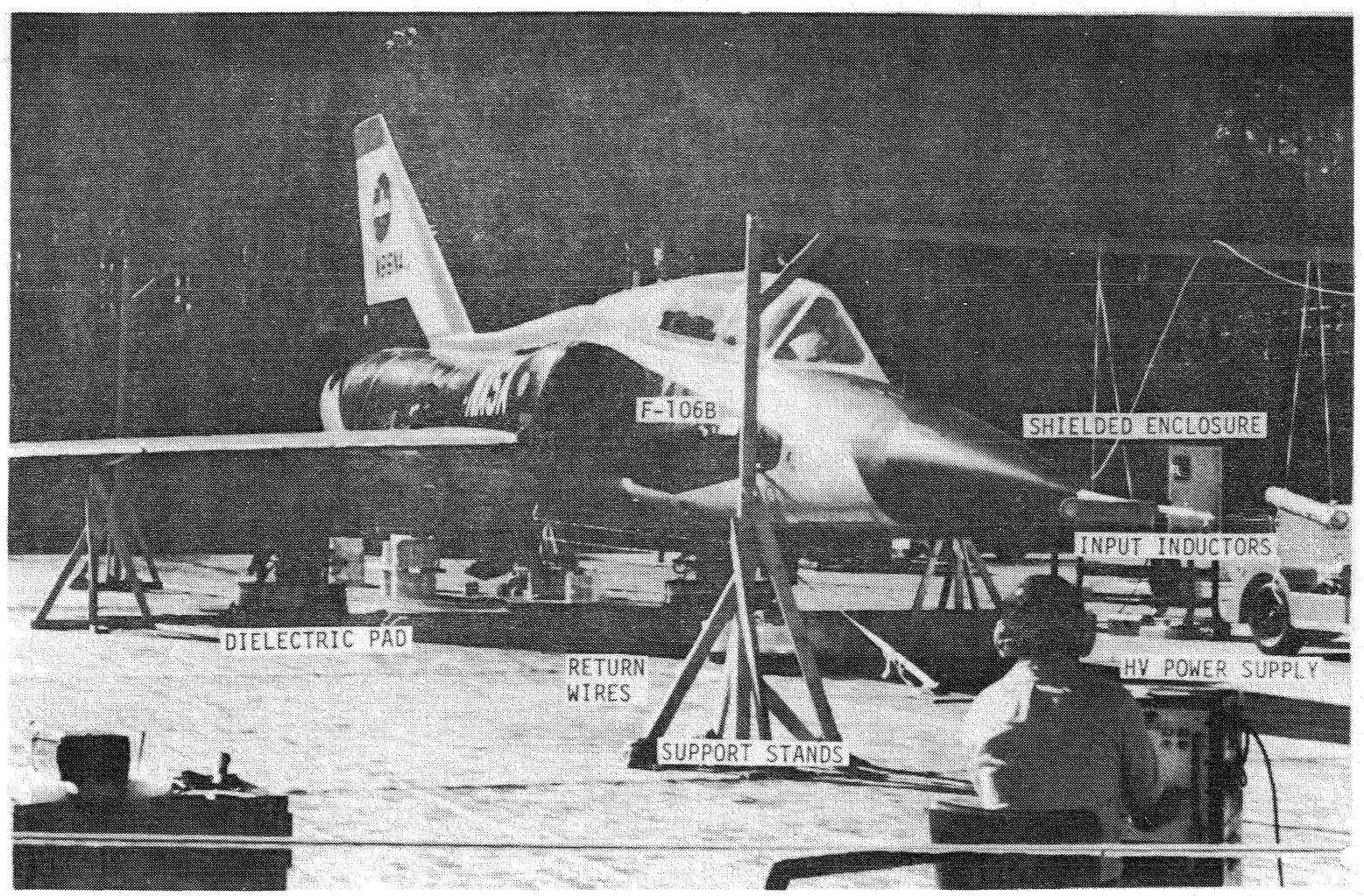

FIGURE 3 - F-106B DIRECT ATTACHMENT TEST SETUP

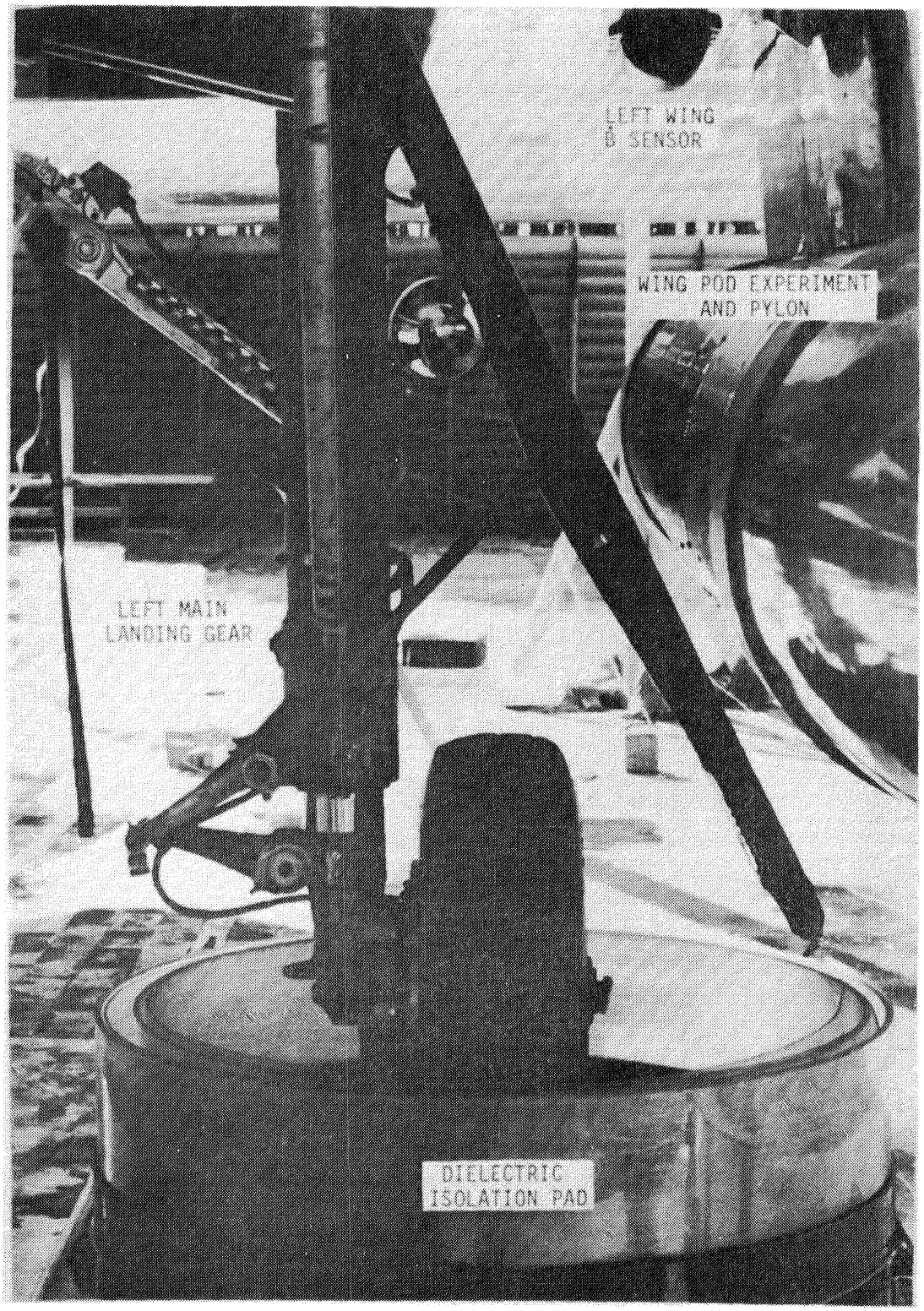

FIGURE 4 - LEFT MAIN LANDING GEAR ON A DIELECTRIC ISOLATION PAD

FIGURE 4

and the "coaxial" return wire system was constructed. The return wire system consisted of four groups of three #12 wires located approximately 10 feet from the fuselage.

Six stages of the modular Marx generator system were mounted horizontally on a support stand outside the nose end of the aircraft/return wire transmission line. The output from the Marx generator system was routed over the forward wooden support structure to the pitot tube of the aircraft. The low-voltage side of the generator was connected directly to the junction of the return conductors. The generator system and return conductors were completely isolated from earth ground before firing by an air-actuated, oil-filled charge/dump system.

The input stimulus to the aircraft was varied by connecting the generator output directly to the aircraft or by adding either of two coil inductors (50, 200 μH) before the aircraft connection. The coils increased the system inductance and thereby affected the current and voltage rise times applied to the aircraft. The output from the aircraft was a single 12-gauge wire to the aft junction of the current return lines. The aircraft output locations were varied during the test. Connections from the tail hook beneath the engine outlet and the right and left wing tips were used.

For many of the tests, a spark gap consisting of two separated 2.0-inch copper spheres was inserted in the output line about 3 feet from the aircraft output connection. With the spark gap in the output, the aircraft was first charged to a high-potential by displacement currents and then discharged as the output spark gap broke down. The spark gap distance was varied during some of the testing.

Test data were gathered using a computer-controlled data acquisition system located in an RFI shielded enclosure. The sensor or wire responses were

transmitted from the aircraft to the shielded enclosure using MCAIR-designed fiber optic data links with a bandwidth of 25 MHz. Inside the enclosure, the data were reconverted to their electrical equivalents and recorded by transient digitizers. The data were then analyzed as desired and stored on magnetic tape cassettes.

Test data were gathered from both NASA aircraft sensors and MCAIR sensors. Table 1 is a listing of all the sensors used in the test program. On each shot either the system current or the aircraft voltage was measured using MCAIR sensors. In addition, other MCAIR $\dot{B}$ and $\dot{D}$ sensors were taped to the aircraft exterior in the vicinity of NASA sensors, so that both the NASA and MCAIR sensors could be monitored simultaneously to provide comparative responses. Some of the MCAIR sensors were designed for "free-field" measurements and were located on a rotatable dielectric support about 10 inches above the metal aircraft exterior to prevent pertubation of the measurement. Figure 5 shows a typical sensor placement (without the fiber optic transmitter) near the NASA $\dot{B}_{TRANSVERSE}$ sensor on the left side of the aft upper fuselage.

The NASA sensors and interior wires were monitored at the input to the aircraft instrumentation package inside the missile bay. In many cases the same sensor output was monitored by both the NASA on-board system and our remote system by using a six-decibel power splitter to evenly divide the sensor output voltage to the 50Ω NASA recorder input and our terminated fiber optic transmitter. Other standard 50Ω attenuators were inserted before the power splitter to adjust the sensor output levels to the recorders.

The MCAIR transmitters used to monitor the NASA sensors were located inside the missile bay and were connected to the sensor's coaxial line (with attenuators) by a short length of coaxial cable. The fiber optic cables were routed back to the receivers in the shielded enclosure through an air vent in the missile bay door.

TABLE 1 - MCAIR AND NASA SENSORS

MCAIR SENSORS	CONVERSION FACTOR $\left(\frac{\text{OUTPUT VOLTS}}{\text{UNITS OF MEASURED PARAMETER}}\right)$
$\dot{B}$ -- EG & G MGL-6	1×10^{-3}
$\dot{D}$ -- EG & G HSD-4	1.0
$\dot{D}$ -- EG & G CFD-1	5×10^{-2}
I -- PEARSON 3025	1.25×10^{-2}
$\dot{I}$ -- EG & G CPM-1	1×10^{-8}
V -- HAEFFLY	7.23×10^{-4}
NASA SENSORS	
$\dot{B}$ -- FUSELAGE	5.73×10^{-3}
$\dot{B}$ -- WING	5.5×10^{-3}
$\dot{D}$ -- FUSELAGE, TAIL	2.0
D -- WING TIPS	1.35
$\dot{I}$ -- NOSE	2.1×10^{-9}
I -- NOSE	0.195
I -- FUSELAGE WIRE	5.0

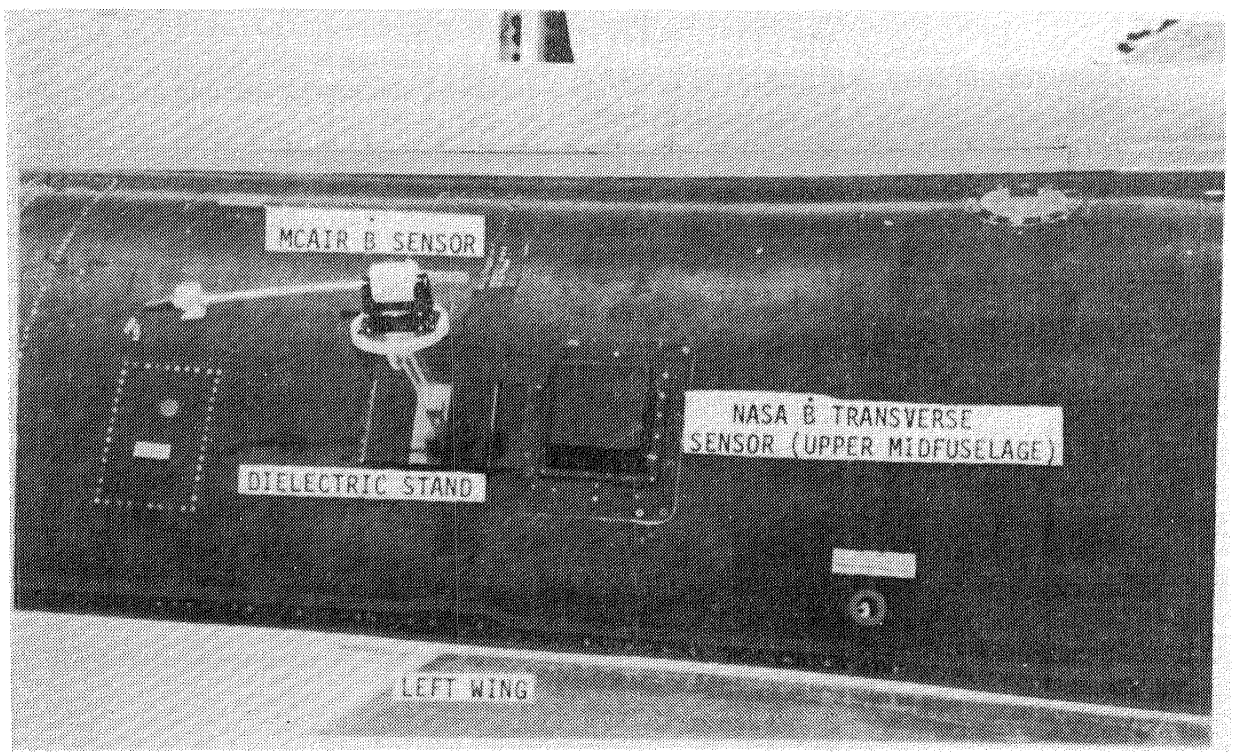

FIGURE 5 - TYPICAL MCAIR $\dot{B}$ SENSOR PLACEMENT

TABLE 1 AND FIGURE 5

3.2 RADIATED TEST SETUP. Figure 6 is a schematic of the radiated test configuration which was designed by Dr. D. V. Giri of Lutech Incorporated using available MCAIR components. The intent of these tests was to excite the isolated aircraft with a radiated electromagnetic pulse to determine the characteristic aircraft resonances. The return conductor assembly and all other long conductors in the vicinity of the aircraft were removed prior to these tests. The aircraft was left on the dielectric isolation pads to help decouple it from ground potential.

The pulse source was the modular Marx generator fired into a 100-m-long by 40-m-wide transmission line. The transmission line was elevated to the height of the wings and was positioned so that the electric field between the two long conductors was parallel to the axis of the aircraft. A long multistranded graphite fiber conductor (with a resistance of 8 Ω/ft) was used to terminate the far end of the transmission line in its characteristic impedance of 1250 ohms. Terminating the transmission line prevented reflections from the two-wire line from interfering with the natural aircraft resonances.

For these tests the aircraft was unpowered, and measurements were made with the missile bay door both open and closed. The four NASA $\dot{D}$ sensors were monitored to yield the aircraft response. The current, current derivative, and the horizontal electric field near the aircraft were measured to characterize the source pulse. All measurements were made with the MCAIR fiber optic data links and instrumentation system. No measurements could be made with the NASA instrumentation system, since aircraft power is needed for its operation. Multiple shots were recorded for each sensor output to determine the extent of the shot-to-shot variation.

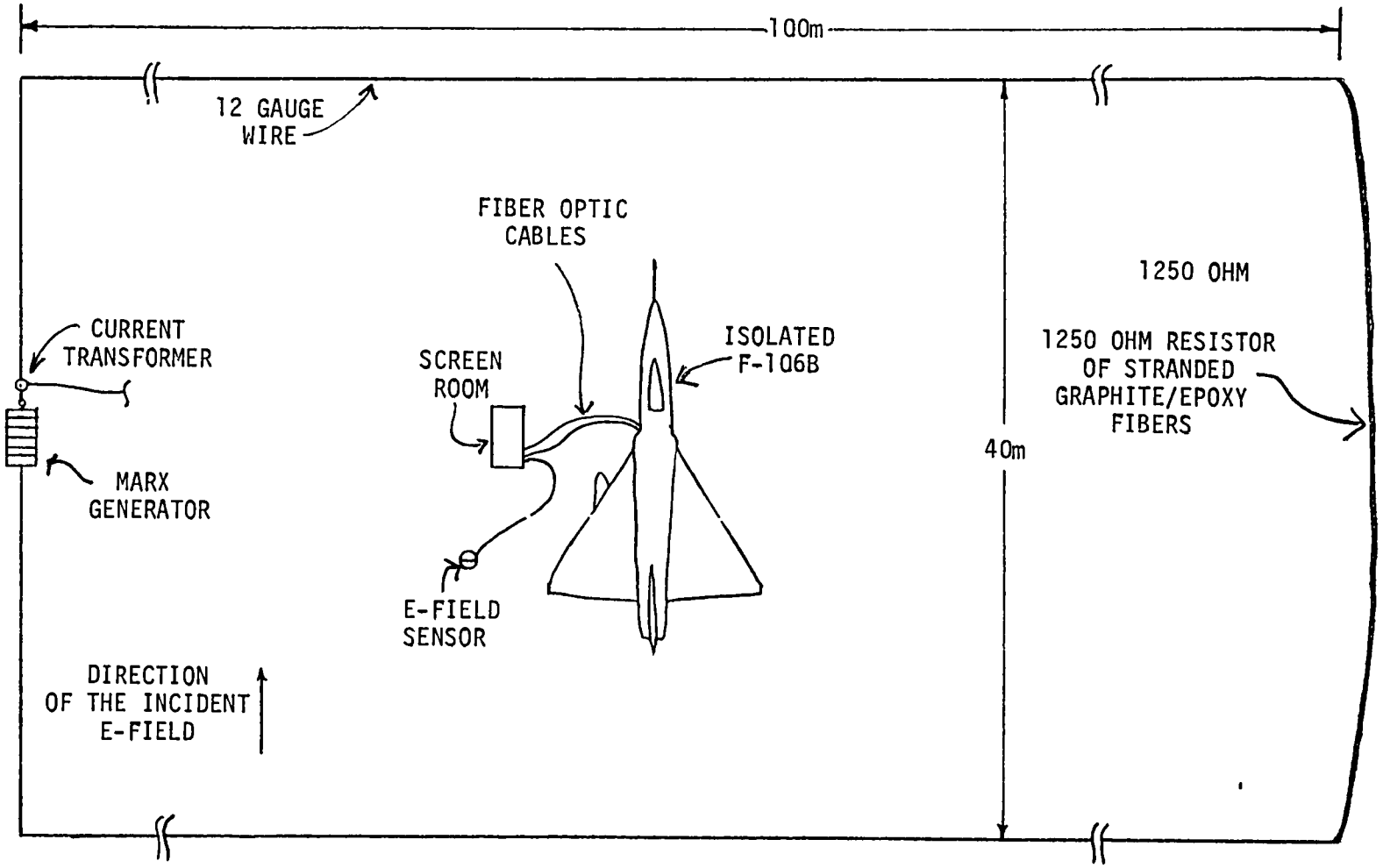

FIGURE 6 - SCHEMATIC OF RADIATED TEST SETUP

FIGURE 6

4.0 TEST PROCEDURE

Most of the F-106B lightning tests were conducted with the pilot and flight engineer in the cockpit and the engine running. Only the sensor output level tests of the first day and the radiated tests on the last day were run with the aircraft unpowered. The tests monitored various combinations of NASA sensors, interior wires, and MCAIR sensors for many different test conditions to include: (1) direct attachment or radiated stimulation, (2) different system inductances and, therefore, different input waveforms, (3) different output locations (tail hook, left wing tip, right wing tip), (4) hard-wired or spark gap output, (5) different spark gap distances, and (6) the effect of an added output inductance. Generally only one parameter was changed at a time to establish a cause-and-effect relationship between sequential shots. In addition, two identical shots were conducted for most variations to establish the repeatability of the data.

The test procedure was the same regardless of the test variation being studied. Each morning, and whenever a fiber optic channel was changed, a calibration of the entire data acquisition system was completed by inputting a known amplitude sawtooth waveform into each channel. Thereafter all recorded signals were scaled in amplitude by comparison to the calibration level and were then multiplied by the amount of attenuation added between the sensor output line and the fiber optic transmitter. Once the fiber optic transmitters were connected to the interior NASA sensor lines, the NASA ground support crew closed the missile bay doors, and the pilot started the aircraft engine. Before each test shot, the MCAIR data system was armed, and the aircraft's flight engineer was notified to ready the NASA instrumentation system. After the shot, the NASA package was placed in a standby condition, and the MCAIR data was observed and recorded on magnetic tape. External system changes were

readily made between test shots by MCAIR personnel. When it was necessary to monitor different NASA sensors, the ground support crew opened and secured the missile bay doors and made the necessary attenuator level and connection changes. The doors were then closed and testing continued. The aircraft engine was shut down only during lunch and after the day's testing was completed.

5.0 DIRECT ATTACHMENT TEST RESULTS

During the one-week test program, 164 total test shots were recorded. One hundred thirty-nine of these shots were conducted with the aircraft in the coaxial test configuration connected directly to the high-voltage Marx generator. For most shots, four channels of data were recorded by the MCAIR instrumentation system, and two channels each were monitored on the NASA transient recorders and NASA wide-band analog recorder. To completely analyze and compare these data is a major task that would require several months of effort. The purpose of this section is to demonstrate the various types of data that were measured and to summarize the results observed on a first pass through only the MCAIR data.

Representative data traces in the time domain and their fast Fourier transforms (FFT) in the frequency domain are presented in this report. NASA Langley has previously been provided with a complete data set that includes copies of all test shots, the daily data log, and a sequence-by-sequence summary of the test results. NASA also intends to transfer the recorded digital data from the MCAIR cassettes to their magnetic tape storage system for subcontractors and their own future use.

This section first overviews the time domain data and then discusses the frequency domain characteristics of the direct attachment test data. Section 6.0 discusses the results of the radiated tests.

5.1 TIME DOMAIN DATA. Many different combinations of MCAIR and NASA sensor responses were recorded during the tests. A maximum of five data channels could be recorded by the MCAIR instrumentation system, but damage to one of the Biomation 6500's limited most of the testing to four transient recorder channels. At times five sensors were monitored and the data were recorded on

two successive shots by switching the input leads to the other Biomation 6500.

The data to be summarized here are subdivided into five categories depending on the test parameters varied and whether the data were obtained in a single shot or multiple shots. Virtually every data channel of the 139 shots can be compared in some way to every other data channel. Some of the different types of comparison are discussed in the following paragraphs.

5.1.1 Same Test Shot, Different Sensors. Figure 7 shows a typical test shot with the aircraft output hard-wired from the tail hook to the junction of the return conductors. (The second trace was actually measured on an identical shot and has been inserted in the trace location of the damaged transient recorder channel.) The system current is a damped sinusoid with a peak of 2.8 kA and frequency of ≈330 kHz. The calculated system inductance is 42 μH. The induced voltage and current of the interior fuselage wire are shown in the top two traces. These two waveforms have very similar waveshapes and are related in magnitude by the 50Ω monitoring resistance in the circuit. The fuselage wire transients are phase shifted by 90° from the system current as expected for inductive coupling in the common mode circuit. $\dot{B}$ transients were monitored with MCAIR sensors on the access door aft of the nose gear (on the lower forward fuselage) and on the upper fuselage near the NASA $\dot{B}_{TRANSVERSE}$ SENSOR. The two waveforms demonstrate that most of the current flow is in the axial direction; however, a fast transverse component is present immediately after the generator is triggered. The peak $\dot{B}$ of 1800 T/s at the lower forward fuselage location agrees fairly closely to the 1500 T/s calculated for a uniform current distribution on the nose perimeter forward of the cockpit.

Figure 8 shows a typical test shot with a spark gap inserted between the aircraft output connection and the return wire conductors. In this test configuration, the aircraft is first charged by displacement currents and then

TEST 3/30Y

INDUCED VOLTAGE ON THE FUSELAGE WIRE
(WIRE SHORTED AT FORWARD BULKHEAD)

INDUCED CURRENT ON THE FUSELAGE WIRE
(MEASURED NEAR THE MID-POINT OF THE WIRE'S LENGTH)
(THIS TRACE FROM TEST 3/30V)

SYSTEM CURRENT
(MEASURED IN OUTPUT WIRE NEAR THE TAIL HOOK)

$\dot{B}$ (LOWER FORWARD FUSELAGE)
MCAIR SENSOR - RESPONDS TO AXIAL CURRENT DENSITIES

$\dot{B}$ (TRANSVERSE, UPPER FUSELAGE)
MCAIR SENSOR - RESPONDS TO TRANSVERSE CURRENT DENSITIES

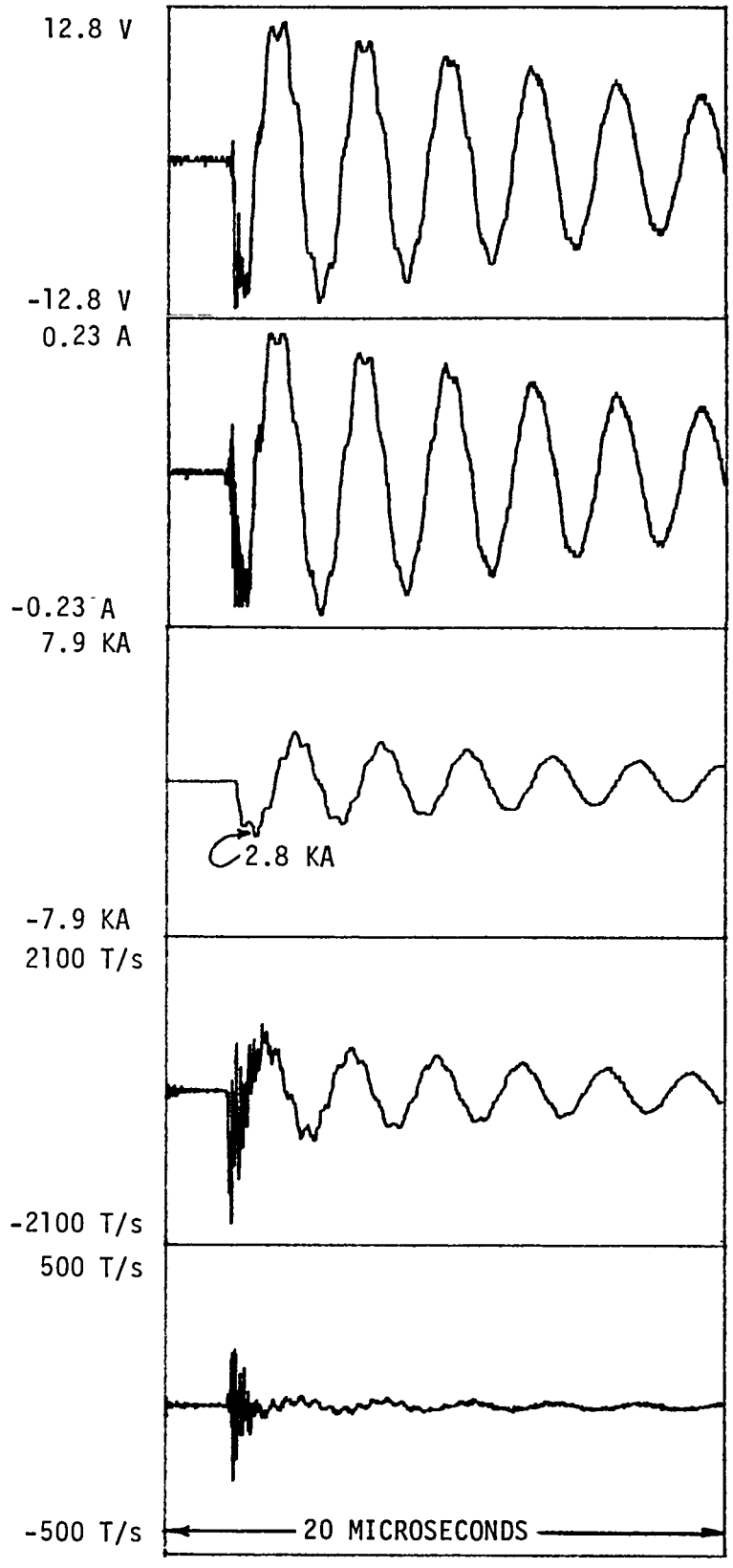

FIGURE 7 - TYPICAL SHOT WITH HARD-WIRED OUTPUT, NO ADDED INDUCTANCE, OUTPUT FROM THE TAIL HOOK

FIGURE 7

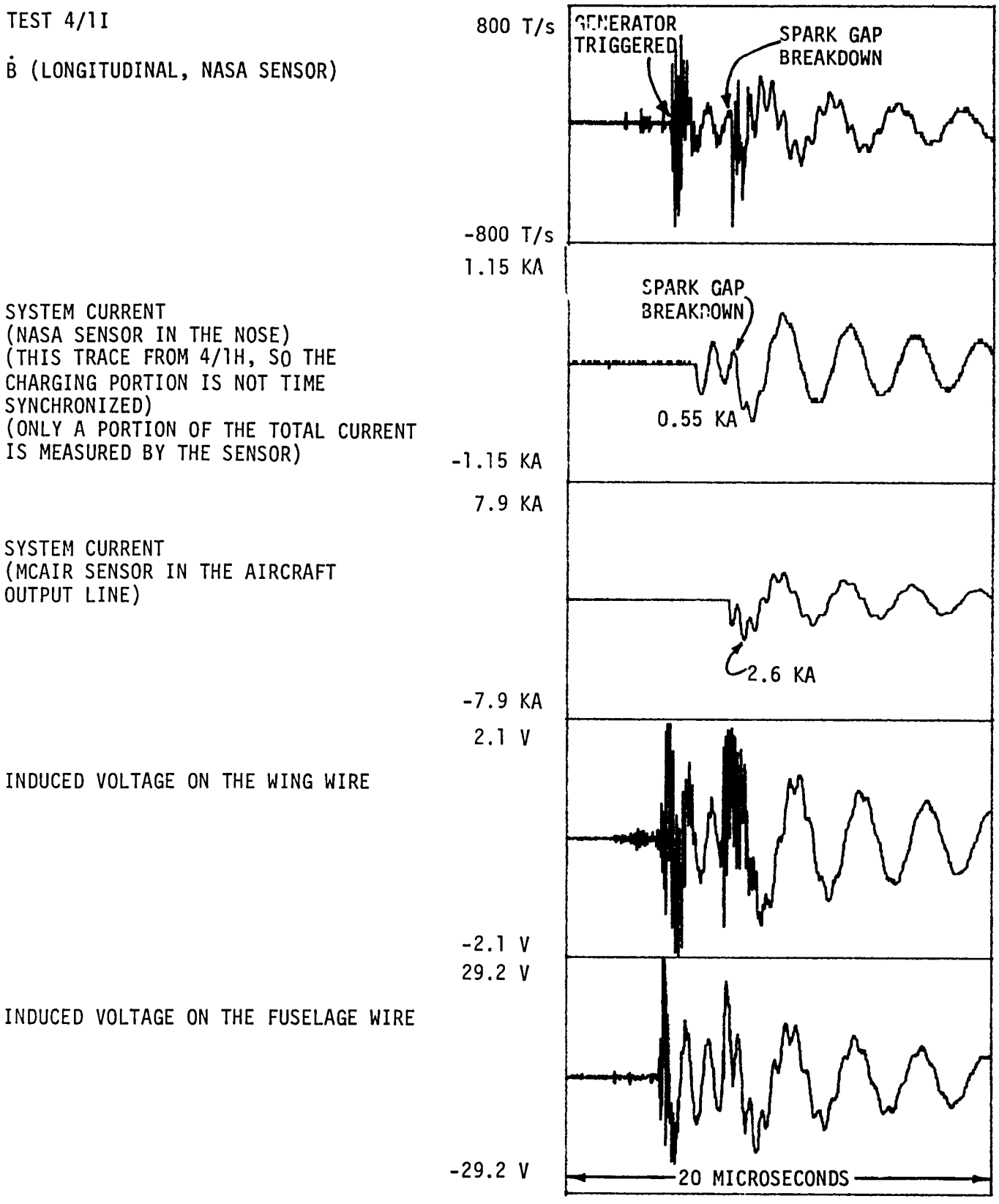

FIGURE 8 - TYPICAL SHOT WITH A SPARK GAP IN THE OUTPUT 10-INCH ARC, NO ADDED INDUCTANCE, OUTPUT FROM THE TAIL HOOK

FIGURE 8

discharged when the spark gap breaks down. The second and third traces show the system current as measured in the nose and the output. The current measured in the nose shows the displacement currents that flow to charge the aircraft-to-return conductor capacitance. The current measured in the output contains only the discharge current which is modulated by a setup dependent transmission line frequency at ≈2 MHz. Both the induced voltage responses have approximately equal peak magnitudes before and after the output arc. The coupling to the wing wire is about 15 times less than that of the fuselage wire. The NASA $\dot{B}_{LONGITUDINAL}$ sensor on the upper fuselage displays the derivative of the fields produced by both the charging and discharge currents. The $\dot{B}$ sensor and interior wires contain some quickly damped high frequency content at the generator triggering and spark gap breakdown. This high frequency content is due to the natural aircraft resonances and is discussed in the frequency domain section.

Figure 9 is a comparison of the NASA and MCAIR $\dot{D}_{VERTICAL\ STABILIZER}$ for a 4-inch output spark gap. During the first three days of testing, MCAIR sensors were positioned near the NASA sensors and their responses compared. In general, the waveform shapes and magnitudes were in good agreement. The $\dot{D}$ responses throughout the aircraft contained strong oscillations at the ≈2 MHz system resonances even with the output hard-wired. When an output spark gap was used, the amplitude of the oscillations increased as the aircraft was charged to a high potential before the spark gap broke down. For the short 4-inch spark gap used in Figure 9, the aircraft is quickly discharged when the spark gap breaks down after one-quarter of a displacement current oscillation.

Figure 10 compares the MCAIR $\dot{B}$ sensor responses for a system configuration

TEST 3/30DD

$\dot{D}$ (VERTICAL STABILIZER)
(NASA SENSOR)

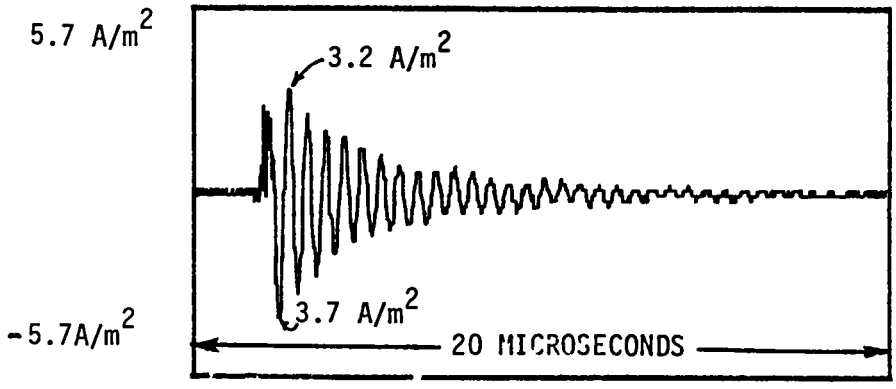

(THE TRACE INVERSION IS DUE TO OPPOSITE SENSOR DIRECTIONS BEING USED IN THE MEASUREMENTS.)

$\dot{D}$ (VERTICAL STABILIZER)
(MCAIR SENSOR HSD-4
10 INCHES FROM SURFACE)

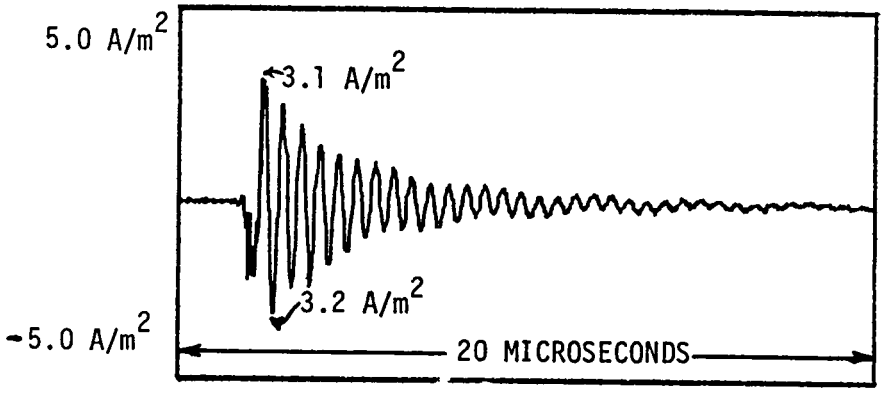

FIGURE 9 - COMPARISON OF NASA AND MCAIR $\dot{D}$ SENSOR; NO ADDED INDUCTANCE, 4" ARC, TAIL OUTPUT

FIGURE 9

TEST 3/30P

$\dot{B}$ (LOWER FORWARD FUSELAGE)
(MCAIR SENSOR → RESPONDS
TO AXIAL CURRENT DENSITIES)

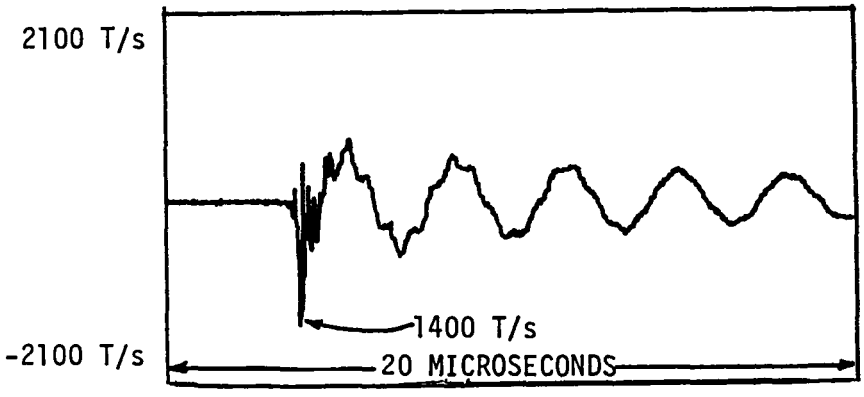

(THE TRACE INVERSION IS DUE TO OPPOSITE
SENSOR DIRECTIONS BEING USED IN THE
MEASUREMENTS.)

$\dot{B}$ (UPPER MID-FUSELAGE)
(MCAIR SENSOR → RESPONDS
TO AXIAL CURRENT DENSITIES)

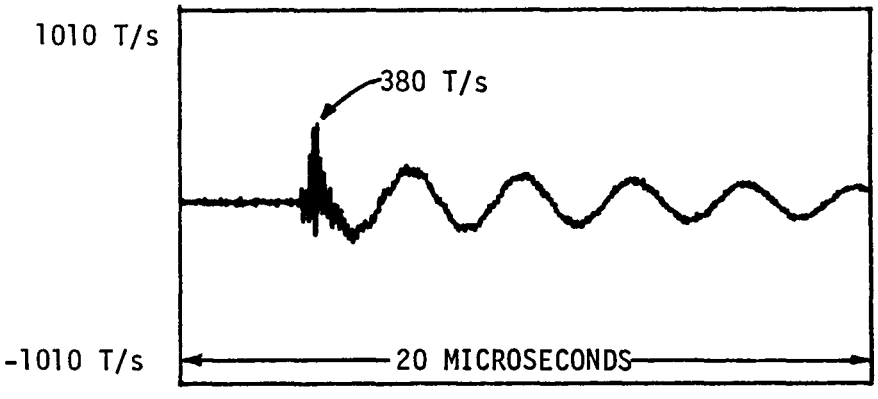

FIGURE 10 - COMPARISON OF MCAIR $\dot{B}$ SENSOR RESPONSE AT TWO LOCATIONS,
NO ADDED INDUCTANCE, HARD-WIRED OUTPUT FROM THE LEFT WING TIP

FIGURE 10

with a hard-wired output connection from the left wing tip to the junction of the return conductors. The lower forward fuselage $\dot{B}$ has a peak amplitude of 1400 T/s which closely agrees with the calculated 1500 T/s. The peak longitudinal $\dot{B}$ response on the upper mid-fuselage is only 380 T/s. These and similar results for the tail output show that the current density near the NASA longitudinal sensor is only one-quarter of that on the forward fuselage. The increased fuselage diameter and added surface area of the delta wing effectively spread the current distribution to produce the smaller current density.

Figure 11 compares the response of the NASA $\dot{B}$ sensors on the wings for a spark gap output from the tail. Since the aircraft and test setup were symmetric about the aircraft's axis, a nose-input-to-tail-output test configuration should produce like responses on the wing sensors. Figure 11 demonstrates one shot for which the magnitudes and waveshapes are nearly identical.

5.1.2 Same Sensors for Different Output Locations. Figure 12 shows the response of MCAIR $\dot{B}$ sensors on the right wing and upper mid-fuselage for hard-wired outputs from the tail and the right wing tip. The MCAIR sensors were located near and oriented like the NASA $\dot{B}$ sensors. The upper fuselage sensor responds to axial (longitudinal) current flow down the fuselage, and the wing sensor responds to transverse current flow from wing to wing. With the output at the tail, the transverse current flow in the wing is small at the slow system frequency. With the output at the right wing tip, the system current must flow across the wing and produces the larger transverse component response. Except for an initial spike, the longitudinal current flow on the fuselage sensor remains at approximately the same amplitude for either output location. The fuselage sensor response contains more modulation at 2 MHz for the tail output.

TEST 4/1Q

$\dot{B}$ (LEFT WING)
(NASA SENSOR → RESPONDS TO
TRANSVERSE CURRENT DENSITIES)

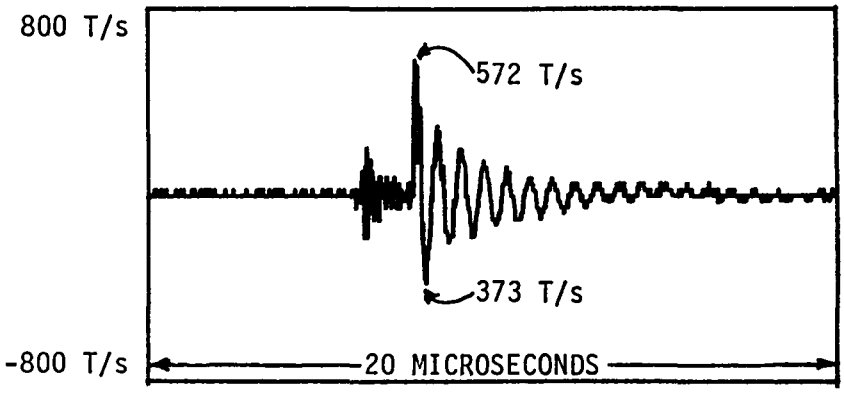

$\dot{B}$ (RIGHT WING)
(NASA SENSOR → RESPONDS TO
TRANSVERSE CURRENT DENSITIES)

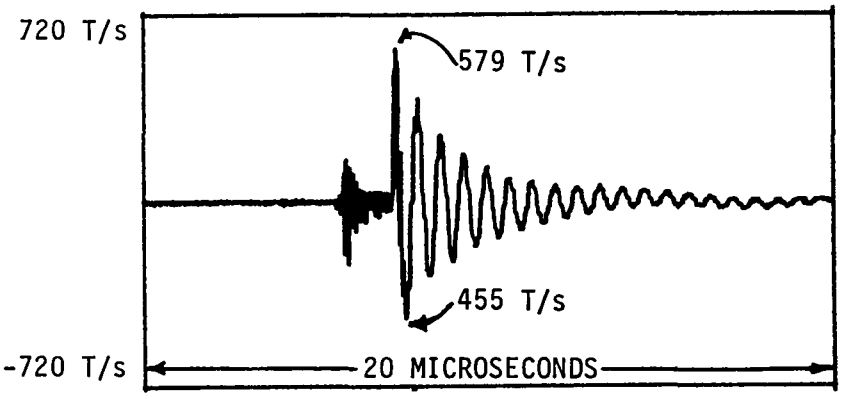

FIGURE 11 - COMPARISON OF COMPLEMENTARY NASA SENSORS, 10-INCH SPARK GAP IN THE TAIL OUTPUT, 200 μH ADDED INDUCTANCE

FIGURE 11

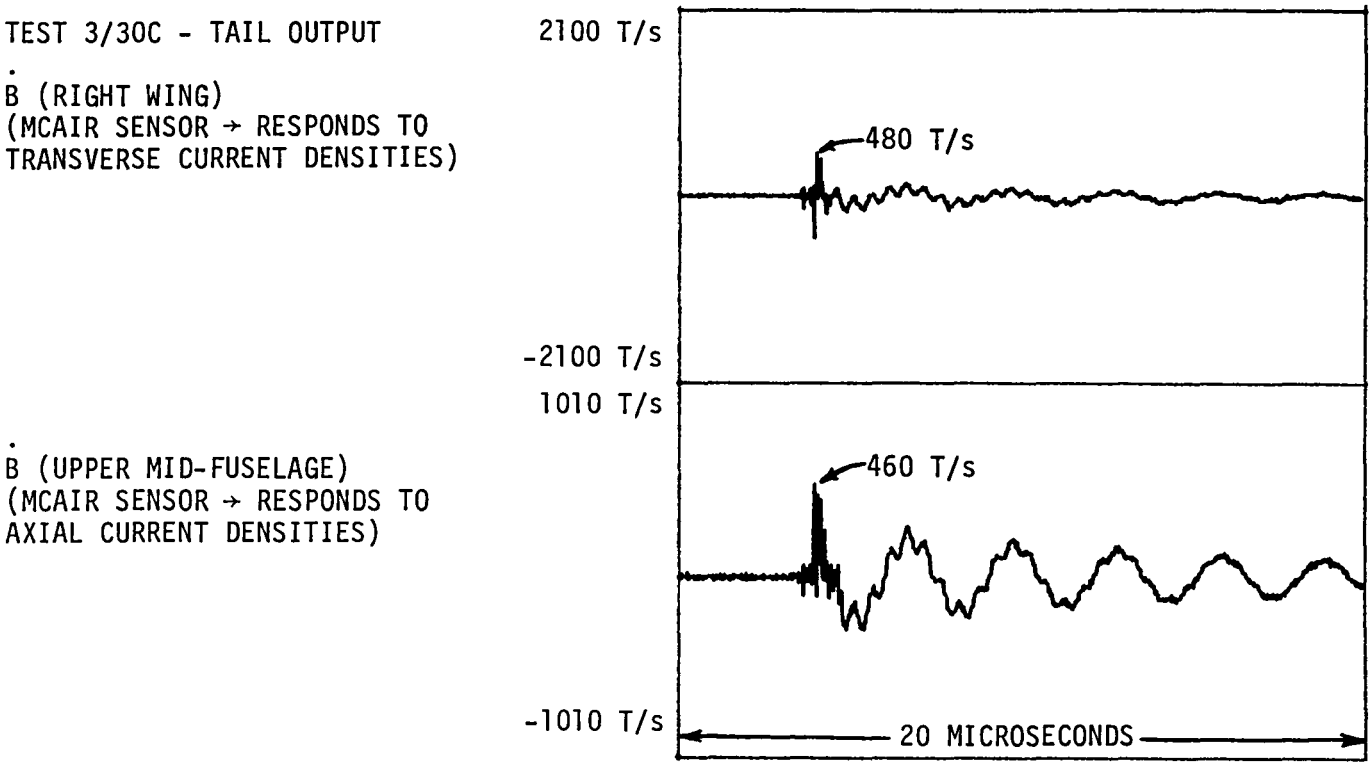

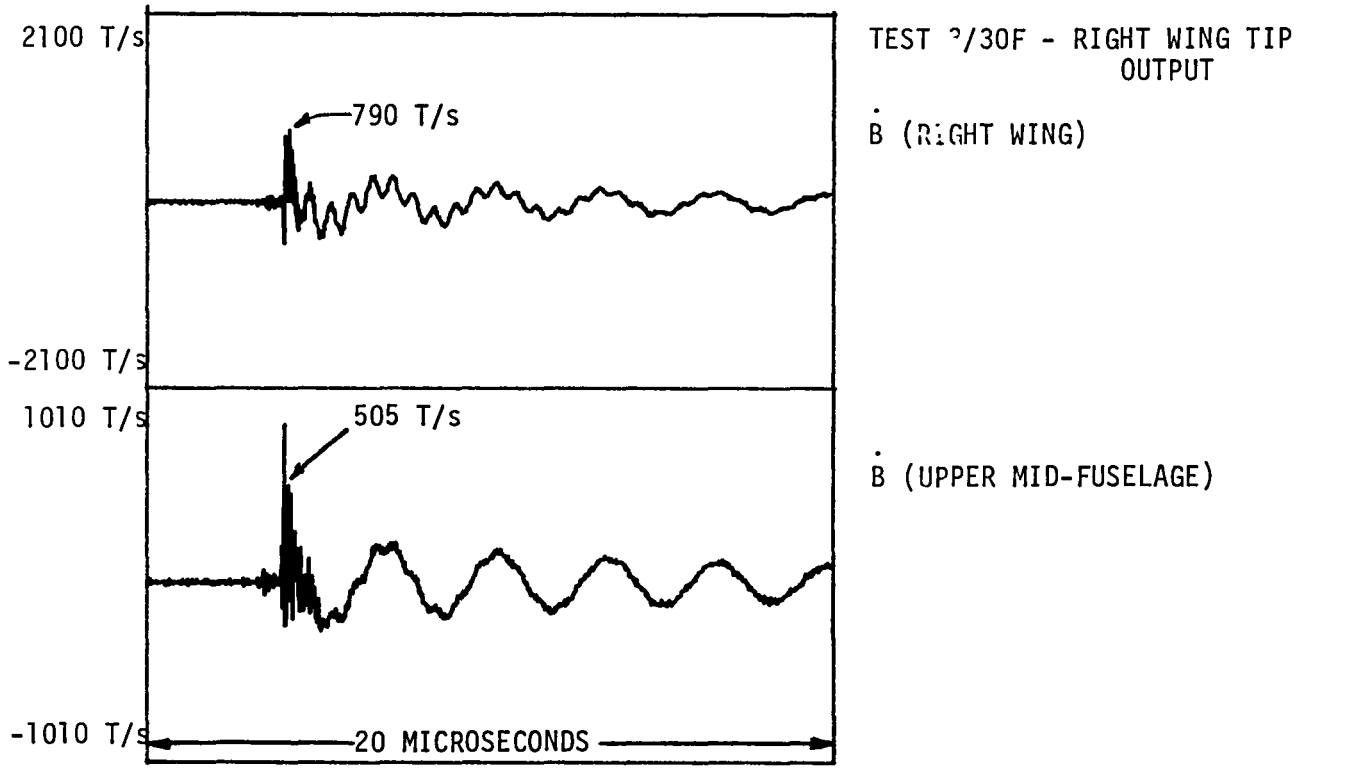

FIGURE 12 - COMPARISON OF $\dot{B}$ SENSOR RESPONSES FOR DIFFERENT OUTPUT LOCATIONS, HARD-WIRED OUTPUTS, NO ADDED INDUCTANCE

FIGURE 12

5.1.3 Same Sensors for Different System Inductance Levels. Throughout the test program the input system inductance was varied to change the aircraft stimulus in a controlled manner. Many test sequences were run where the only parameter varied was the system inductance. Figures 13 and 14 are two such sequences.

In the test shots shown in Figure 13, a capacitive voltage divider was used to monitor the aircraft voltage while the fuselage wire, NASA's $\dot{B}$ transverse sensor, and NASA's $\dot{D}$ vertical stabilizer sensor were being observed. The frequency compensated capacitive divider monitored the voltage developed across the output spark gap. With the divider in the circuit, both the aircraft-to-return conductor and the divider capacitances are charged prior to the spark gap breakdown. The addition of the divider's capacitance slows the displacement current resonance somewhat, but provides very useful information regarding the time variation of the aircraft voltage and its relationship to the response of the other aircraft sensors.

Without the divider in the circuit, the prebreakdown resonance was 1 MHz, and calculations determine that the aircraft-to-return conductor capacitance is 660 pF. The dividers' known capacitance is also 660 pF. When the divider was added to the system, the resonance was slowed to 750 KHz which agrees exactly with the calculated resonance for the two capacitances being charged by the generator.

When the generator is triggered, a damped sinusoidal displacement current, like that shown in Figure 8, flows to charge the aircraft and divider capacitances in parallel. The voltage across the output spark gap is given by $\frac{1}{C}\int I dt$ where C is the parallel capacitance and I is the displacement current. The voltage trace (see Figure 13a) is a cosine waveform whose midpoint of oscillation is shifted about the steady-state voltage level that would be attained if

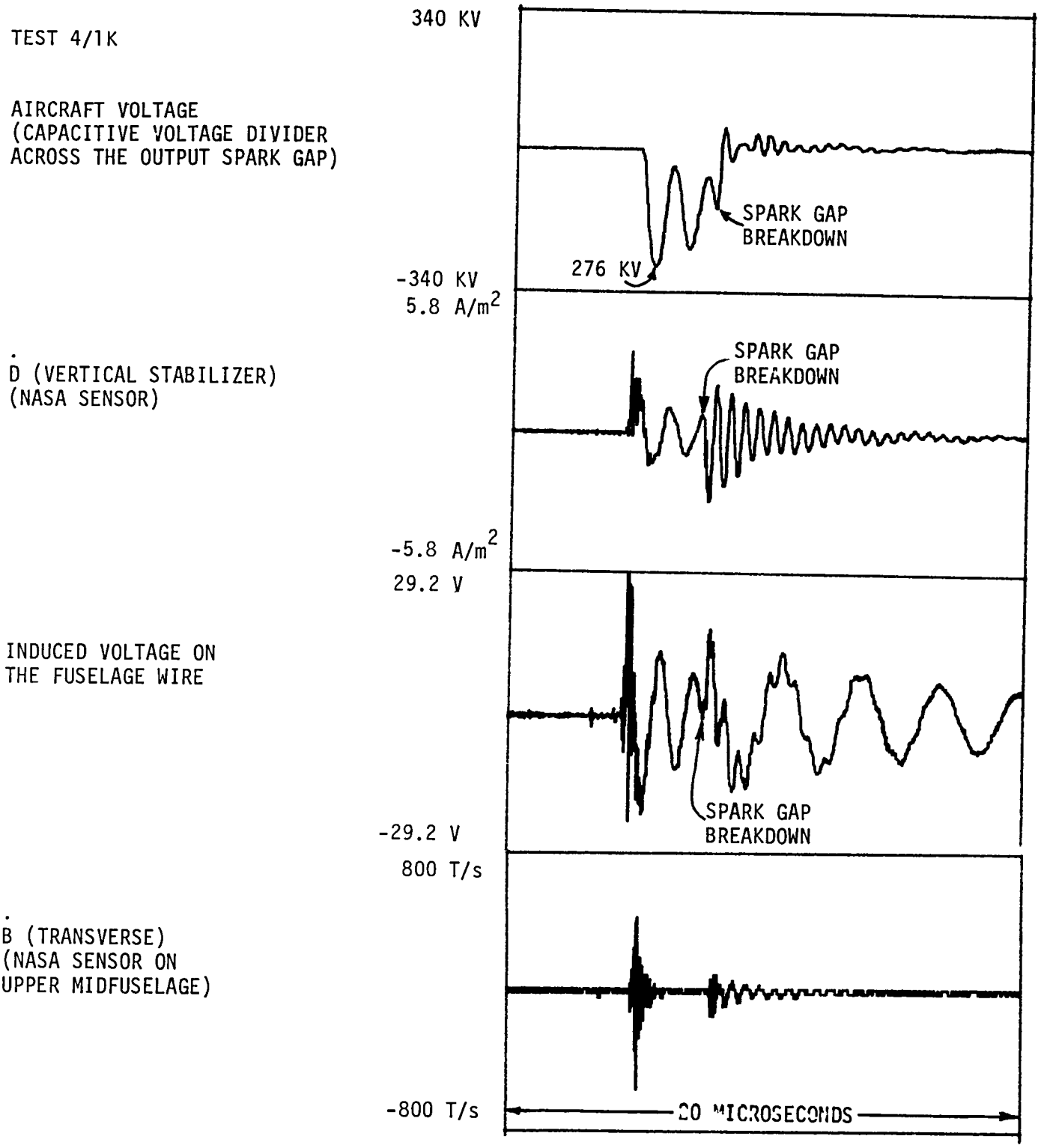

a) NO ADDED INDUCTANCE, L_{TOTAL} = 42 μH

FIGURE 13 - SENSOR RESPONSE VARIATION FOR DIFFERENT SYSTEM INDUCTANCES
(10-INCH SPARK GAP IN TAIL OUTPUT)

FIGURE 13 (cont'd)

(cont'd)

TEST 4/1L

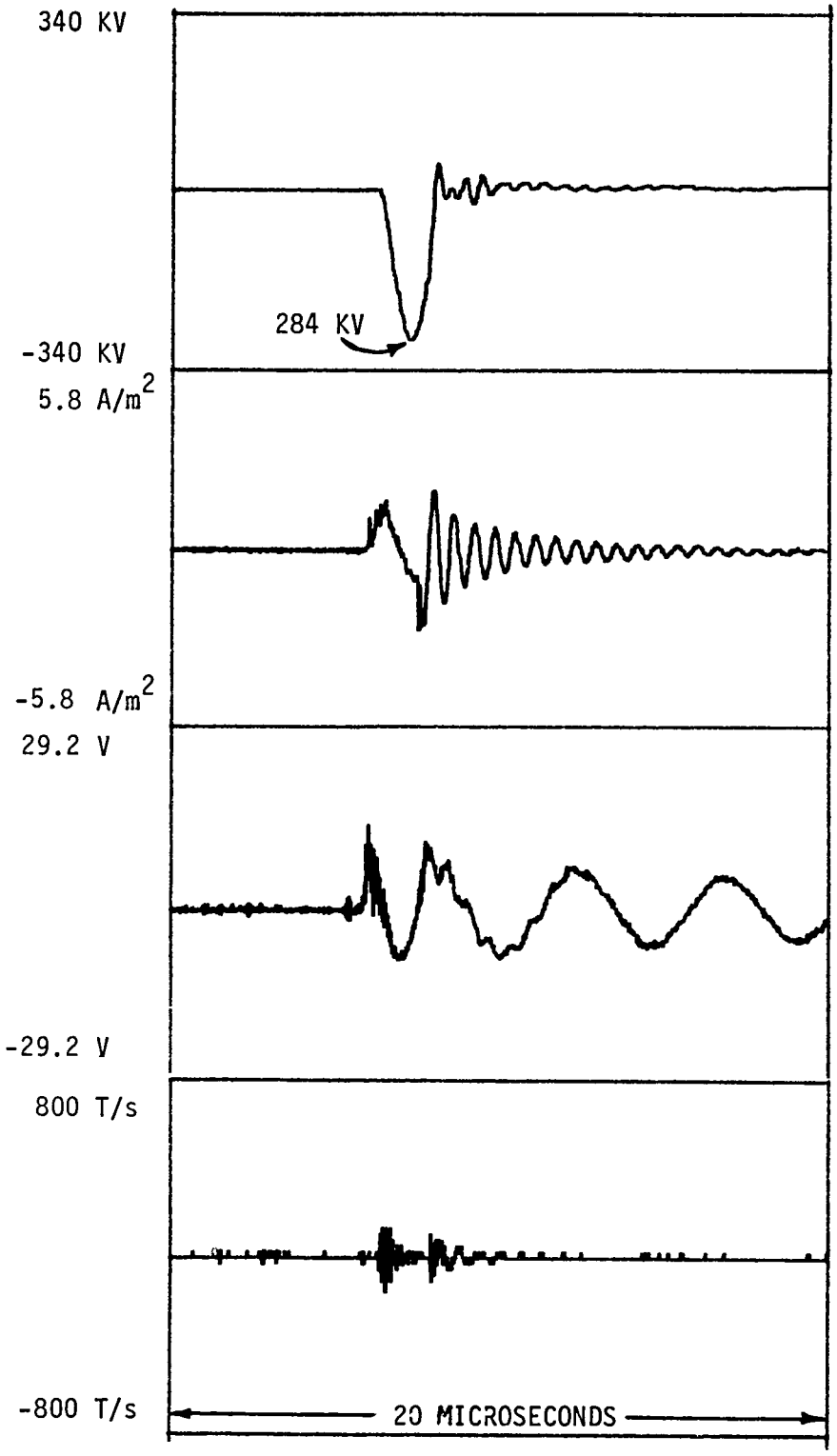

b) 50 μH ADDED INDUCTANCE, L_{TOTAL} = 95 μH

FIGURE 13 (cont'd)

(cont'd)

TEST 4/1M

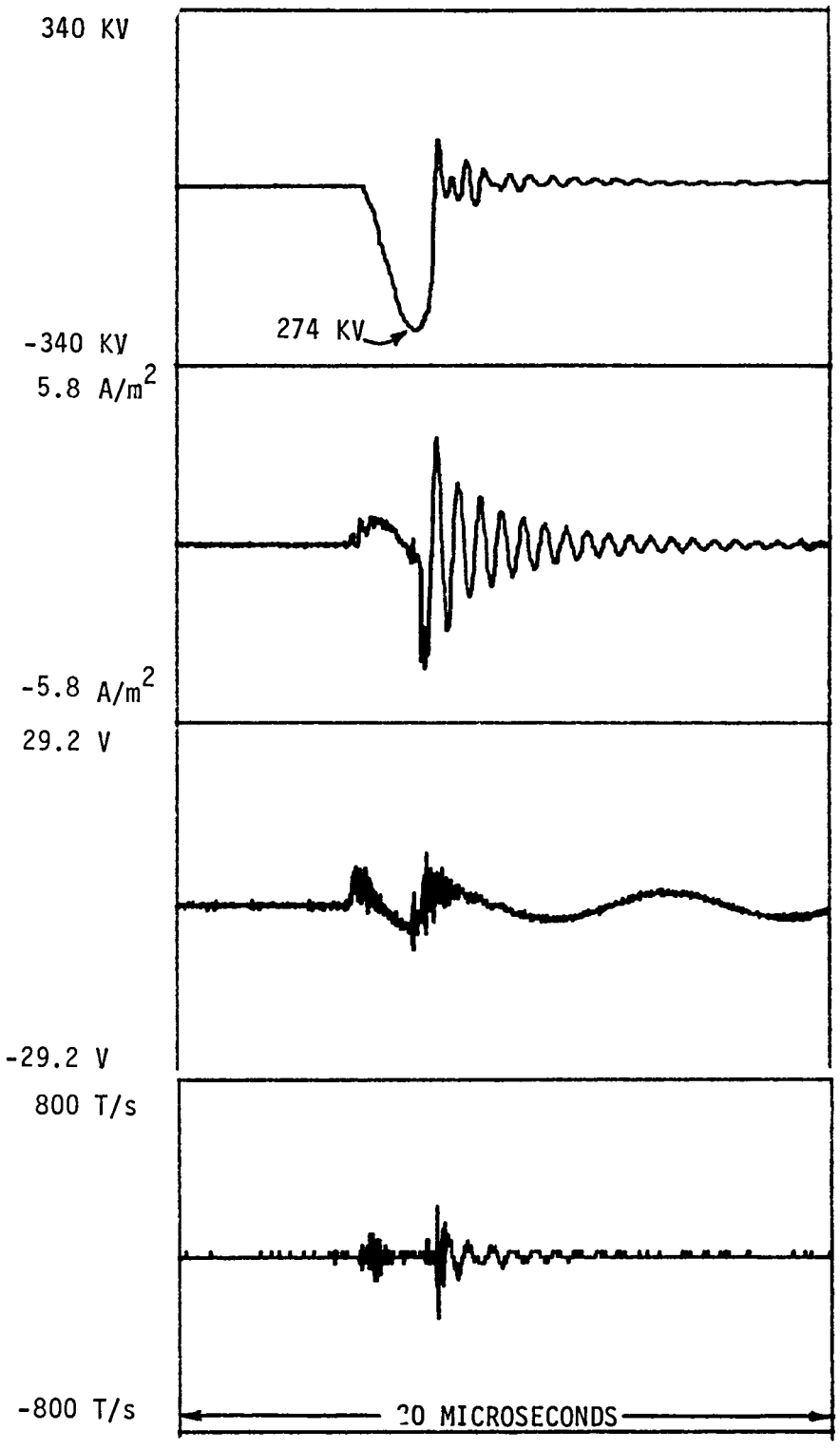

c) 200 μH ADDED INDUCTANCE, L_{TOTAL} = 242 μH

FIGURE 13

TEST 4/1V

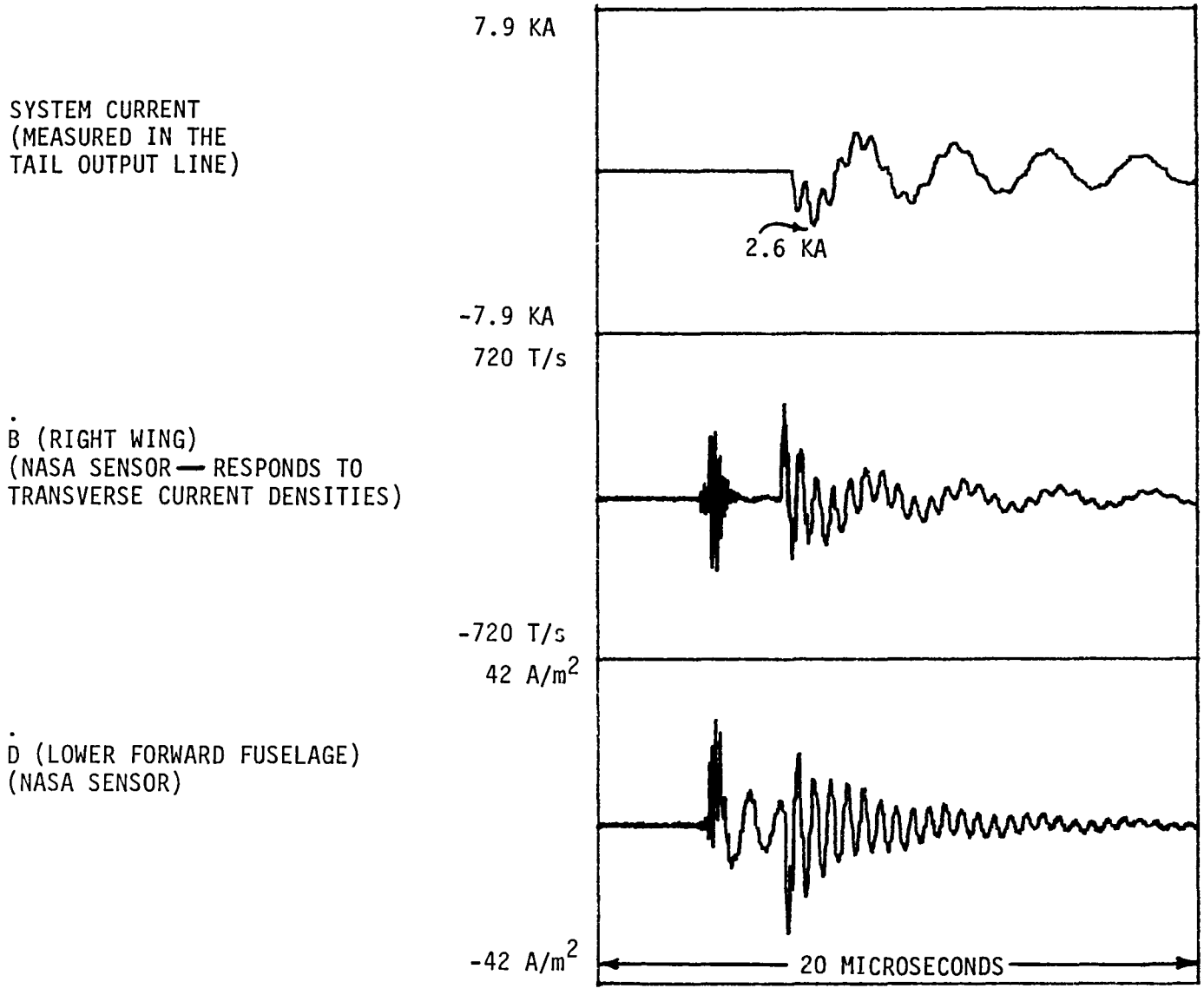

a) NO ADDED INDUCTANCE, L_{TOTAL} = 42 μH

FIGURE 14 - OTHER SENSOR RESPONSES FOR DIFFERENT SYSTEM INDUCTANCES
(10-INCH SPARK GAP IN TAIL OUTPUT)

FIGURE 14 (cont'd)

(cont'd)

TEST 4/1S

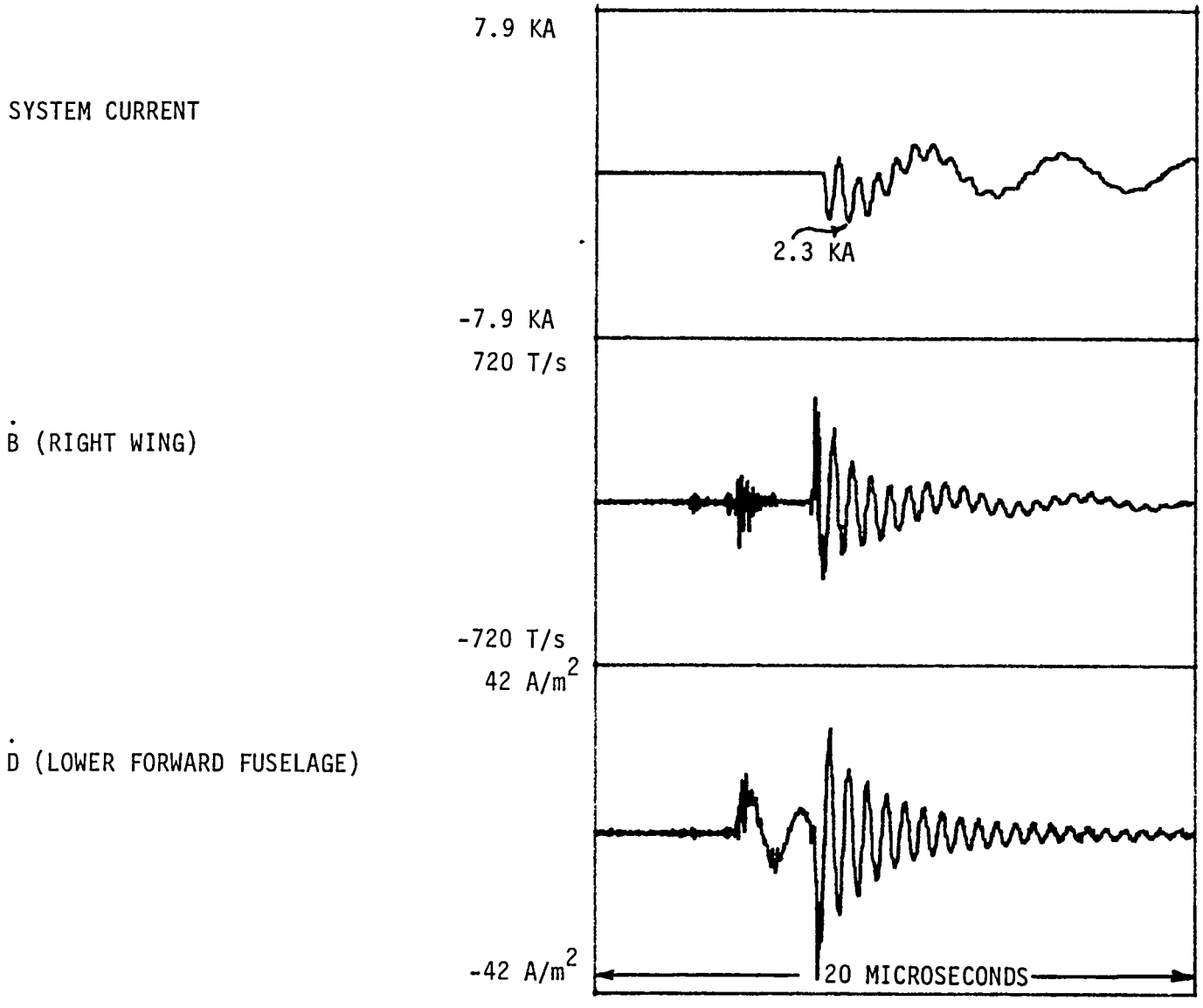

b) 50 μH ADDED INDUCTANCE, L_{TOTAL} = 96 μH

FIGURE 14 (cont'd)

(cont'd)

TEST 4/1R

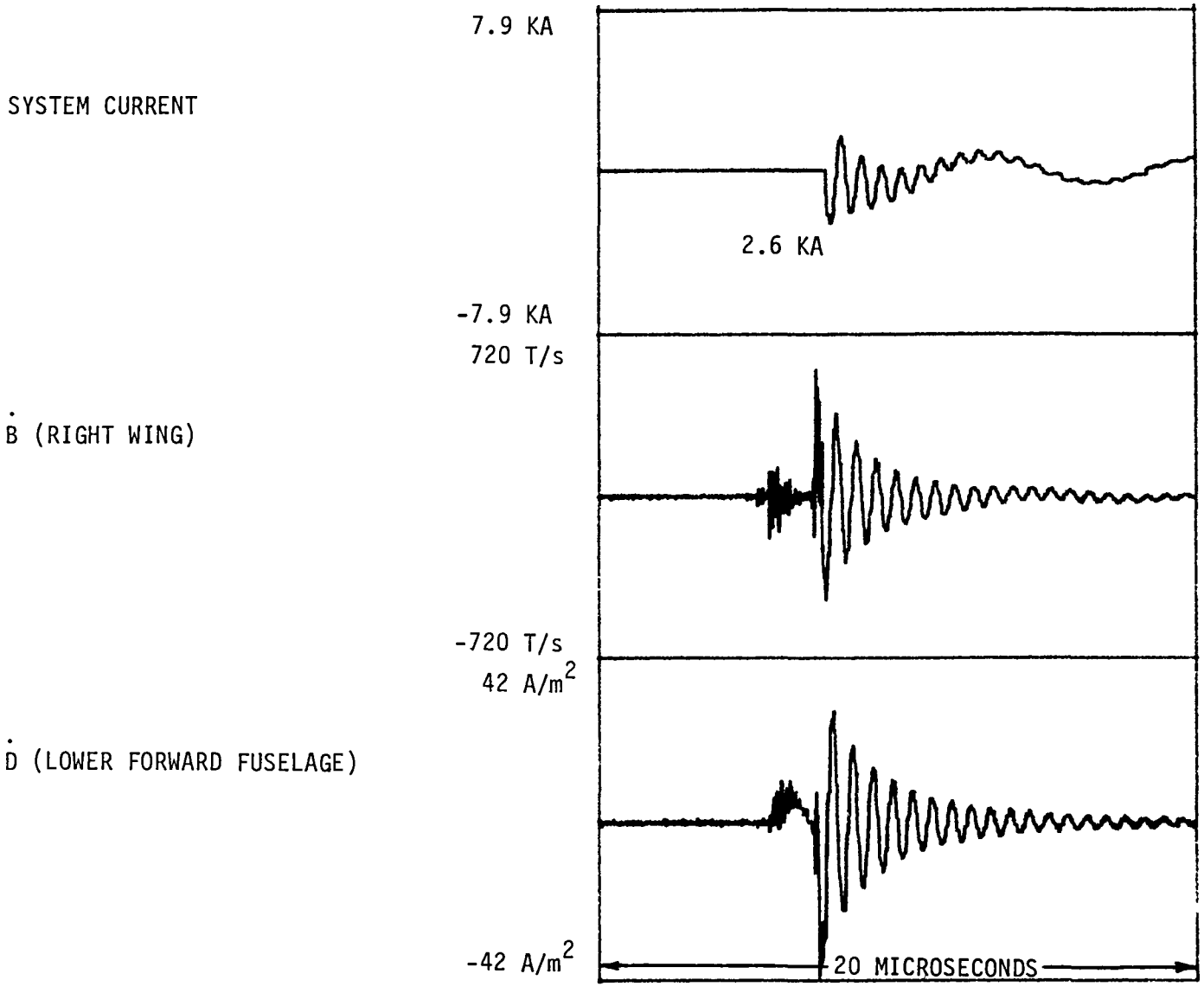

c) 200 μH ADDED INDUCTANCE, L_{TOTAL} = 242 μH

FIGURE 14

the spark gap did not break down. The aircraft reaches its peak voltage (approximately twice the steady-state level) in a half cycle, and the 10-inch spark gap breaks down in 2-1/4 cycles.

Since $D = \varepsilon_o E \alpha V$, $\dot{D}$ is proportional to dV/dt and therefore to I. The sinusoidal response of the vertical stabilizer's sensor is somewhat masked by the high frequency oscillations that occur at generator triggering. However, the fact that in Figure 13a the $\dot{D}$ response is at a maximum after 2-1/4 cycles (when the spark gap breaks down) clearly indicates that the response is sinusoidal and proportional to the displacement currents.

A similar argument (breakdown occurs at a zero point) demonstrates that the induced voltage of the fuselage wire has a cosine response. Such a response is caused by inductive coupling (L dI/dt) to the shorted common mode circuit. The coupling dependence on the current derivative causes the observed 90^{o} phase shift. In circuits where capacitive coupling (C dV/dt) would dominate, the induced voltage response would be in phase with the displacement currents like the $\dot{D}$ sensor response.

The transverse $\dot{B}$ response in Figure 13a shows only the high frequency components at triggering and aircraft discharge. The primary displacement and discharge currents frequencies are not found in the transverse direction on the fuselage.

Figures 13b and c show the response of these same sensors with 50 μH and 200 μH inductors added to the input. The increased inductance limits the rise times of the displacement and discharge currents, and, therefore, slows both resonant frequencies. The slower rise times also cause the magnitude of the derivative sensor's responses to decrease with increased inductance. In addition, the lower charging frequency increases the time that the aircraft is at high voltage and causes the output arc to occur earlier (≈3/4 cycle in Figure 13b

and ≃1/2 cycle in Figure 13c). The system dependence of the $\dot{D}$ sensor and wire responses is again seen in the phase relationships of the waveforms with the added inductance.

Figure 14 presents, for different inductance levels, the responses of the system current in the output, NASA's $\dot{B}$ sensor on the right wing, and NASA's $\dot{D}$ sensor on the lower forward fuselage. The output system current response does not show the displacement currents charging the aircraft. The $\dot{B}$ sensor responds to transverse currents and contains only the high frequency aircraft resonances during charging and a small amount of the basic RLC current response after breakdown. The RLC current variation is dominated by the ≃2 MHz test configuration resonance.

The variation of the $\dot{D}$ sensor transients in Figure 14 clearly shows the slowing of the sinusoidal charging currents and the decrease of the initial peak as the system inductance is increased. In addition, the effect that the time of gap breakdown has on the magnitude of the discharge response is also demonstrated. In Figure 14a, the breakdown occurs near a current maximum which implies that the aircraft voltage is near its steady state level. In Figures 14b and c, breakdown occurs near the current zeros where the aircraft voltage and charge density are the highest. When breakdown occurs, the charge stored on the aircraft is quickly discharged at the test configuration frequency. The larger charge densities just prior to breakdown, therefore, produce larger magnitude $\dot{D}$ responses as the data show. The higher current densities flowing off the aircraft likewise produce increased amplitude discharge current responses on the initial peak of the system current and $\dot{B}$ sensor transients.

5.1.4 Same Sensors for Different Arc Lengths. To restrict the number of variables in the test program, most of the shots were conducted with either a 12-gauge wire connected directly from the aircraft output to the return

conductor junction or with a 10-inch spark gap inserted into the output line to allow the aircraft to charge. However, two short sequences were run in which the monitored sensors were kept the same and the output spark gap distance was varied. Opening the spark gap distance increases the time to breakdown. Since the aircraft charging has a strong oscillatory time dependence, varying the time to breakdown affects the aircraft voltage condition at the time of breakdown. This aircraft voltage variation at breakdown is similar to that described for the case of different inductors except that the charging frequency remains fixed and only the time to breakdown changes.

Figure 15 shows the system current in the output line and the MCAIR lower forward $\dot{D}$ sensor responses for the hard-wired case (no spark gap) and for spark gaps of 4 and 8 inches. The hard-wired system current contains some modulation at the 2 MHz aircraft/return conductor transmission line frequency, but the modulation is much stronger when the spark gap is included in the output. With the spark gap in the line, the transmission line termination is rapidly changed from an open condition to nearly a short circuit when the spark gap breakdown occurs. This termination transition excites current and voltage waves on the aircraft that are reflected back and forth down the transmission line.

This resonance is also evident on the $\dot{D}$ sensor response. With the exception of the initial spike, the hard-wired $\dot{D}$ level is much less than that for the arc cases where the aircraft is charged. Breakdown of the 4-inch arc occurs very quickly so that it is difficult to discern the aircraft voltage condition when breakdown occurred. For the 8-inch arc case, breakdown occurs after 1 1/4 cycles when $\dot{D}$ (and the displacement current) are at a peak and the aircraft voltage would be near its steady-state level. The magnitude of the $\dot{D}$ transient after breakdown for the 8-inch arc is less than that for the 4-inch

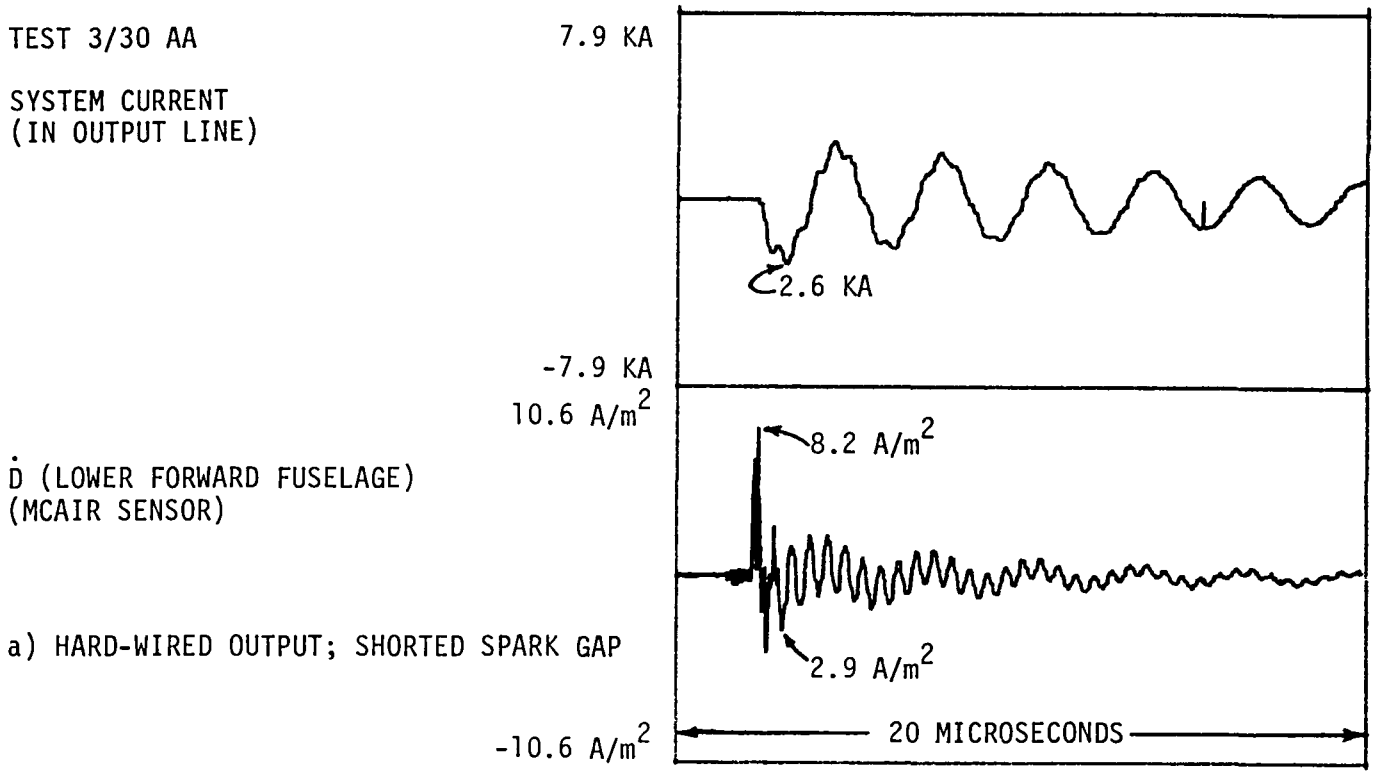

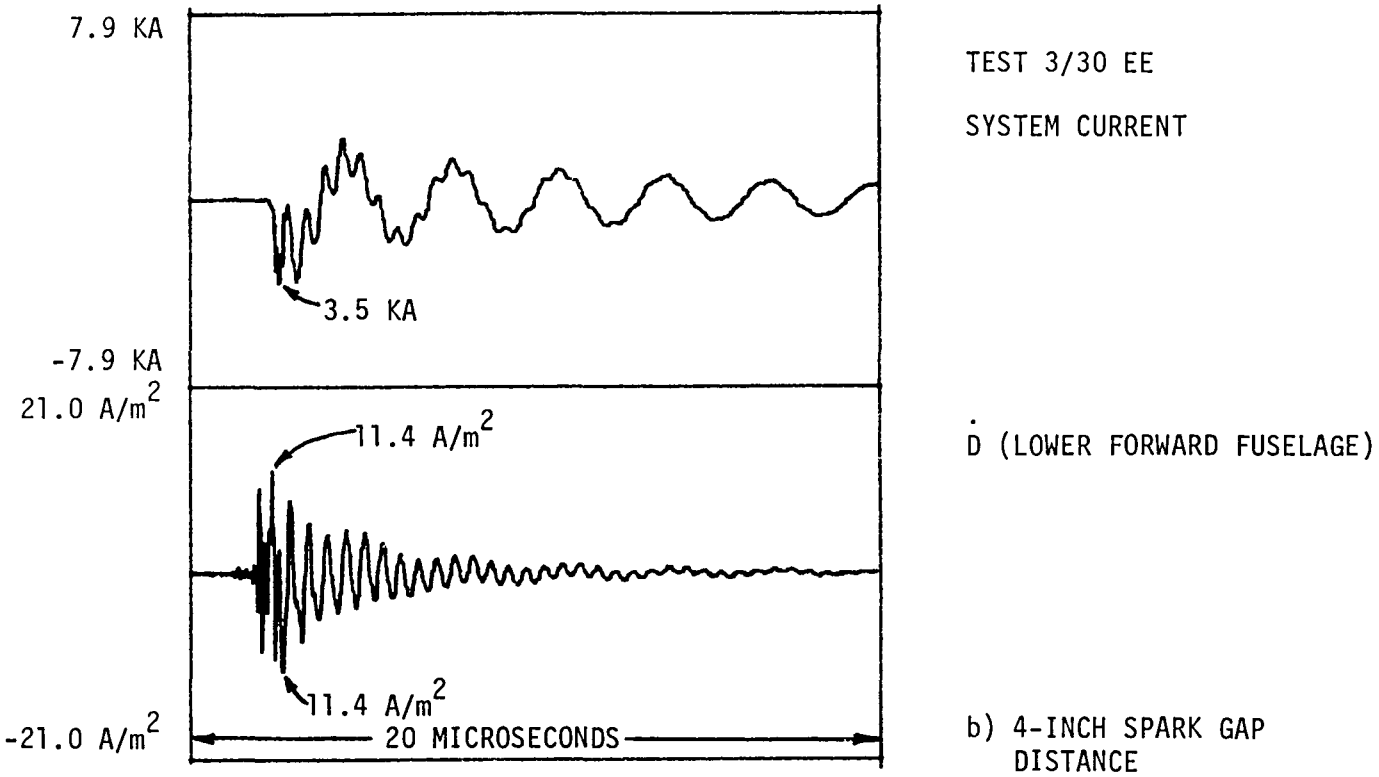

FIGURE 15 - CURRENT AND Ḋ SENSOR RESPONSES FOR DIFFERENT SPARK GAP DISTANCES

FIGURE 15 (cont'd)

(cont'd)

TEST 3/30 HH

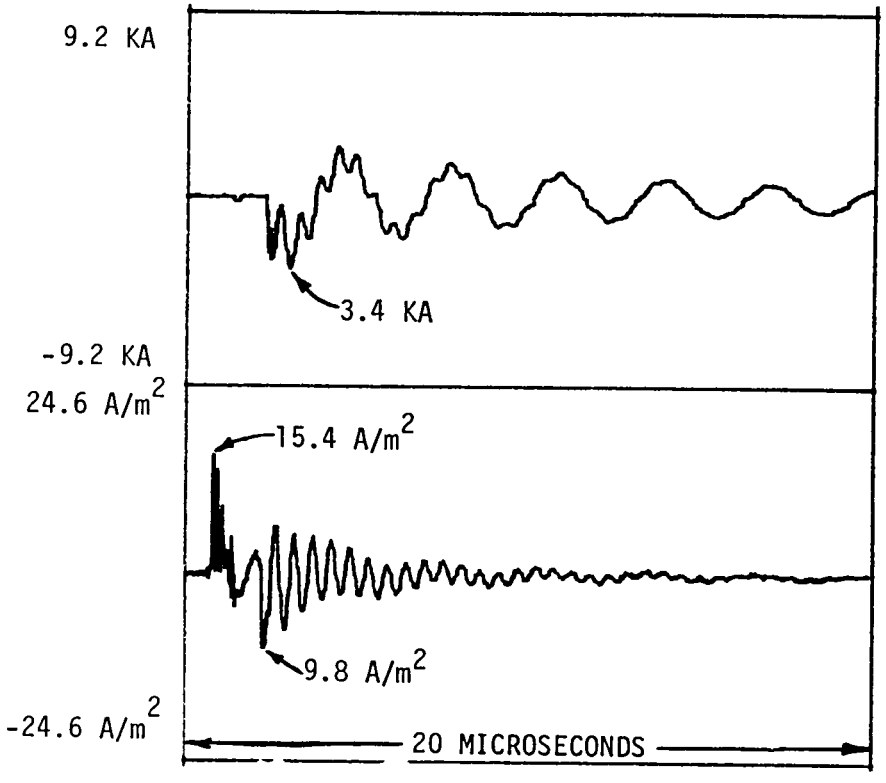

c) 8-INCH SPARK GAP DISTANCE

FIGURE 15

arc which implies that breakdown occurred at a level above the steady-state voltage for the 4-inch arc case.

5.1.5 Same Sensors for Different Input and Output Inductances. The last series of tests conducted for the direct attachment conditions studied the effect of variations in both the input and output inductances on a given set of aircraft sensors. For some of these tests, a 100-μH coil was inserted into the output line in addition to the input inductor variations previously described. This output inductor changes the system resonance somewhat, but, more importantly, it changed the output end termination of the aircraft/return conductor transmission line.

Figure 16 shows the variation of the fuselage wire transient for a hard-wired output and different input and output inductance levels. Note that both the amplitude and frequency of the transmission line modulation of the system response changes for the different terminating conditions. The frequencies of the transmission line modulation were 1.9, 1.6 and 1.5 MHz, respectively, for 0, 50, and 200 μH of added input inductance with no added output inductance. When the 100-μH inductor was added to the output line, these transmission line resonances were shifted to 1.1, .73, and .55 MHz, respectively. The reason for this frequency variation is discussed further in paragraph 5.2.2.

5.2 FREQUENCY DOMAIN DATA. The measured data contain frequencies generated from three sources: the system RLC frequencies during aircraft charging and discharge, transmission line frequencies due to the test setup, and the aircraft's characteristic resonances. The RLC frequencies are dependent on the primary system components and layout. Key elements include the generator capacitance, the aircraft to return conductor capacitance, and the system inductance. The resonant frequencies are readily modeled by a series RLC

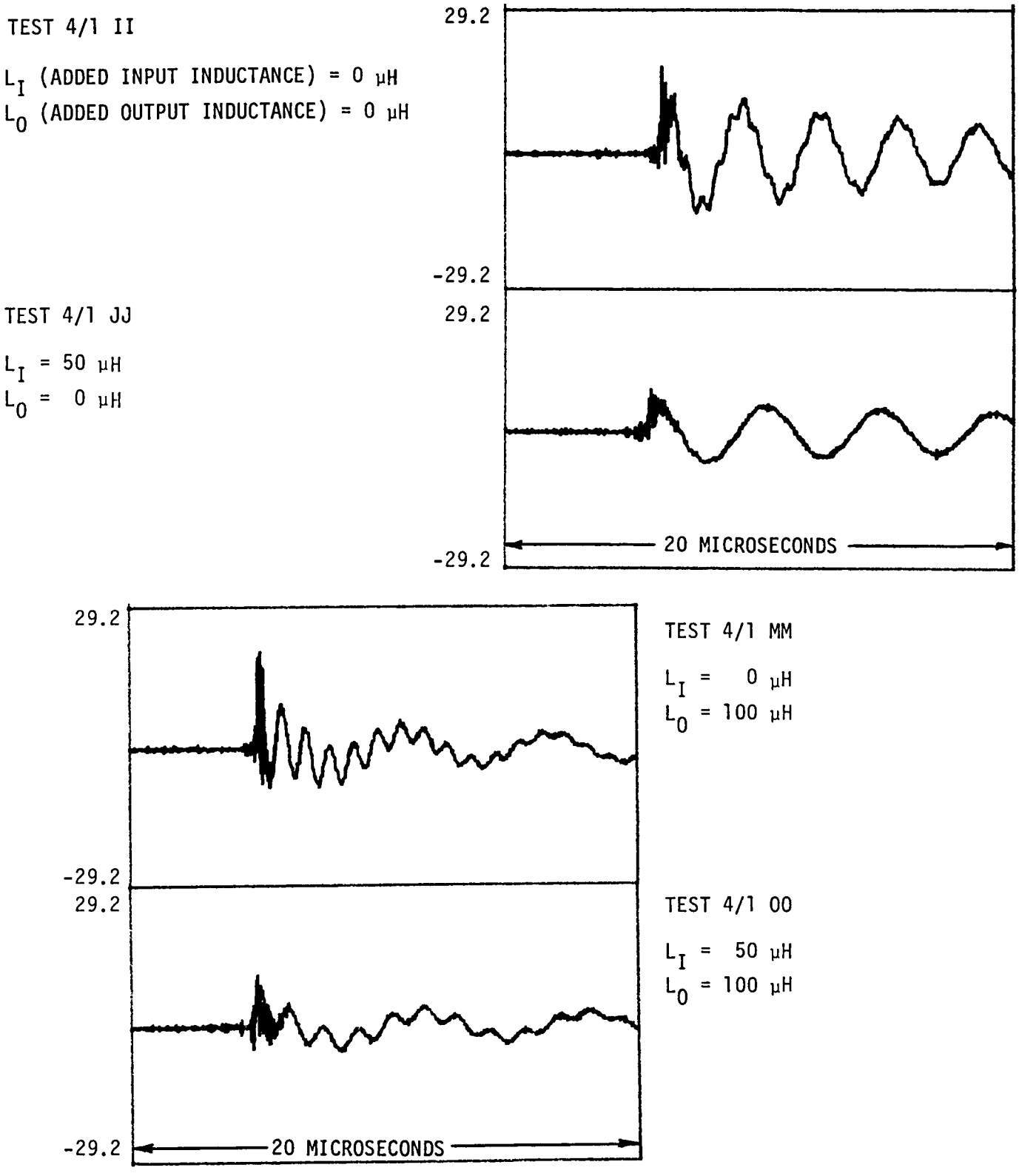

FIGURE 16 - FUSELAGE WIRE RESPONSE FOR DIFFERENT INPUT AND OUTPUT INDUCTANCE LEVELS; (HARD-WIRED OUTPUT)

FIGURE 16

circuit and were varied during the test program by changing the circuit inductance. The transmission line frequencies are principally determined by the physical arrangement of the test setup and the terminations at the ends of the aircraft/return conductor transmission line. Since no resistive elements were intentionally added to the system, there is very little damping of these frequencies. Consequently, the transmission line frequencies (which were varied by changing the input and output inductances) were very strong and dominated the other frequencies during the shock-excitation tests. The aircraft resonances are determined by the physical geometry of the aircraft itself. The high-frequency resonances are excited by abrupt system transitions such as the generator triggering and the spark gap breakdown and are generally damped away in approximately a microsecond.

The characteristic frequencies were identified using a Hewlett Packard fast Fourier transform (FFT) routine that has been incorporated into the data acquisition system software. The FFT provides the power content of the transient as a function of frequency by multiplying the amplitude and phase spectra. The data are normalized to the largest peak and plotted on a linear scale. The routine permits sampling of either 256 or 1024 time domain data pairs. The larger sampling interval provides better frequency resolution, and the smaller sampling interval permits selective analysis of any portion of the transient.

5.2.1 RLC Resonances. The system charging and discharging frequencies are readily modeled as a series RLC circuit. When a spark gap is incorporated in the output, the simple circuit contains both the generator capacitance and the aircraft to return conductor capacitance in series, so that a single equivalent capacitance can be calculated as the series combination of the two capacitances. If the system is underdamped (as in these tests), then the system

RLC resonances can be calculated using $f = 1/2\pi\sqrt{LC}$ where L is the system inductance and C is either the generator capacitance for the discharge case or the series equivalent capacitance for the charging case.

The frequency expression was first used to determine the overall system inductance of 42 μH for the basic system. Then known lumped inductors were added to the system to vary the resonant frequency. The measured frequencies agreed very well with that calculated using the sum of the system and added lumped inductances. The RLC discharge resonances were 330 KHz with no inductance added, 220 KHz with a 50-μH inductor added, and 140 KHz with a 200-μH inductor added.

For the charging or prebreakdown case, the 42-μH system inductance was used to determine the aircraft to return conductor capacitance of 660 pf from the 1 MHz charging resonance. Using this calculated aircraft capacitance, the system was then modified by adding either lumped inductors or the capacitive voltage divider across the output. Again for all cases, the measured frequency agreed well with that calculated using the known lumped values in the basic resonance equation.

5.2.2 Transmission Line Resonances. For a practical test configuration, the aircraft/return conductor transmission line is very nonuniform and difficult to analyze. The terminations at the ends of the line have a large effect in altering the basic transmission line resonance. The explanation of this frequency source will only be briefly summarized here. A detailed study of the resonance is being conducted in the MCAIR independent research and development program (IRAD) using a simple, uniform transmission line test setup.

As shown previously in the data traces, the transmission line frequency (≈2 MHz for the basic F-106B test setup) is present for both the hard-wired and spark gap output configurations. The abrupt transition from an open output

termination to essentially a shorted output termination when the output spark gap breaks down causes the transmission line response to be greatly enhanced for the shock-excitation test technique.

The ideal transmission line resonance can be characterized by its length and terminations. Simple half- or quarter-wavelength resonances are excited for the uniform line with either ideal shorts or opens as end terminations. The practical aircraft transmission line is very nonuniform and the line terminations are not simple opens or shorts, but instead provide some complex impedances that modify the basic resonances. If no resistive elements are incorporated into the terminations, then the terminations are relatively lossless and excite standing waves dependent on their reactances.

For the F-106B test configuration there was appreciable input inductance in the connection of the generator to the input of the aircraft. At frequencies above the RLC resonance, the reactance of this inductance dominates the generators capacitive reactance and makes the input end look like a rather high inductive reactance. As input lumped inductors are added, this reactance increases until the generator end appears almost as an open circuit. The output of the aircraft was connected to the return by a single 12-gauge wire. This wire adds some inductive reactance to the output and, therefore, shifts the termination reactance from that of an ideal short. In previous MCAIR tests where the output connection length was very short and the input inductance was very high, quarter-wavelength resonances have been measured. In this test, the experimental conditions were such that the nonideal terminations caused the system to resonate at frequencies corresponding to electrical line lengths which were much less than a quarter wavelength.

Table 2 shows the calculated phase angles predicted for a given set of input and output impedances. The calculations assume an input inductance of

TABLE 2 - TRANSMISSION LINE FREQUENCIES*

EXPERIMENTAL FREQUENCY (MHZ)	ADDED INDUCTANCE (μH) INPUT	ADDED INDUCTANCE (μH) OUTPUT	TOTAL REACTANCE (Ω) INPUT	TOTAL REACTANCE (Ω) OUTPUT	PHASE ANGLE INPUT	PHASE ANGLE OUTPUT	ELECTRICAL LENGTH	RESONANT FREQUENCY
1.9	0	0	322	179	-65°, 115°	50°	60°	1.7
1.6	50	0	774	151	-79°, 101°	45°	56°	1.6
1.5	200	0	2139	141	-85°, 95°	43°	52°	1.4
1.1	0	100	187	794	-51°, 129°	79°	50°	1.3
.73	50	100	353	527	-67°, 113°	74°	39°	1.1
.55	200	100	784	397	-79°, 101°	69°	32°	.9

*ASSUMES: 90° ELECTRICAL LENGTH = 2.5 MHz, Z = 150Ω,
INPUT INDUCTANCE = 27 μH, OUTPUT INDUCTANCE = 15 μH

27 μH (12 μH for the generator self-inductance and 15 μH for the input line) and an output inductance of 15 μH (for the output line). In addition, the characteristic impedance of the line is assumed to be uniform and is calculated to be approximately 150Ω from the expression ZCc/d = 1 where c is the speed of light, C is the aircraft capacitance of 660 pf, and d is the transmission line length of 100 feet. These assumptions are oversimplified, but they are consistent with the overall system inductance and with the characteristic impedance of approximately 134Ω measured in previous tests using the same setup.

Given these assumptions and the measured experimental frequencies for the different conditions, a set of predicted resonant frequencies is determined by calculating the impedances (X) and the phase angles (arc tan X/150) of the terminations. The portion of a wavelength that can be resonant on the line is the difference of the termination phase angles. The electrical length of the line is then converted to a frequency based on a quarter-wavelength resonance of 2.5 MHz for the 100-foot line. Considering the approximations made, the calculated frequencies compare relatively well with the measured frequencies and show that resonance can occur for frequencies much lower than the quarter-wavelength frequency.

5.2.3 Aircraft Resonances. The high-frequency aircraft resonances are dependent on the aircraft geometry and are excited during abrupt system transitions such as generator triggering and spark gap breakdown. The aircraft resonances are damped very quickly and are, therefore, present during only a small portion of the sampled transient. When the standard 1024 data point FFT routine is used to determine the frequency content of the waveform, the aircraft resonances appear as small secondary resonances because of their small sampling level compared to that of the RLC or transmission line resonances.

Figure 17 shows an example of the time and frequency (1024-point) domain traces of the longitudinal $\dot{B}$ response.

When the FFT routine is limited to 256 data points in the interval where the high-frequency oscillations occur, then the aircraft resonant frequencies are more apparent. Figures 18 and 19 show examples of the high frequency content present in the longitudinal and transverse $\dot{B}$ responses. The primary aircraft resonances occurred at approximately 7, 11, 14, and 18 MHz. The 7- and 18-MHz peaks were present in almost all spectra, while the 11-MHz frequency was primarily present in the longitudinal sensor responses and the 14-MHz frequency was present in the transverse sensor responses. The interior wire responses were inductively coupled to the external fields and, therefore, contained the same high frequency content. Figure 20 shows an example of a wing wire response and spectra.

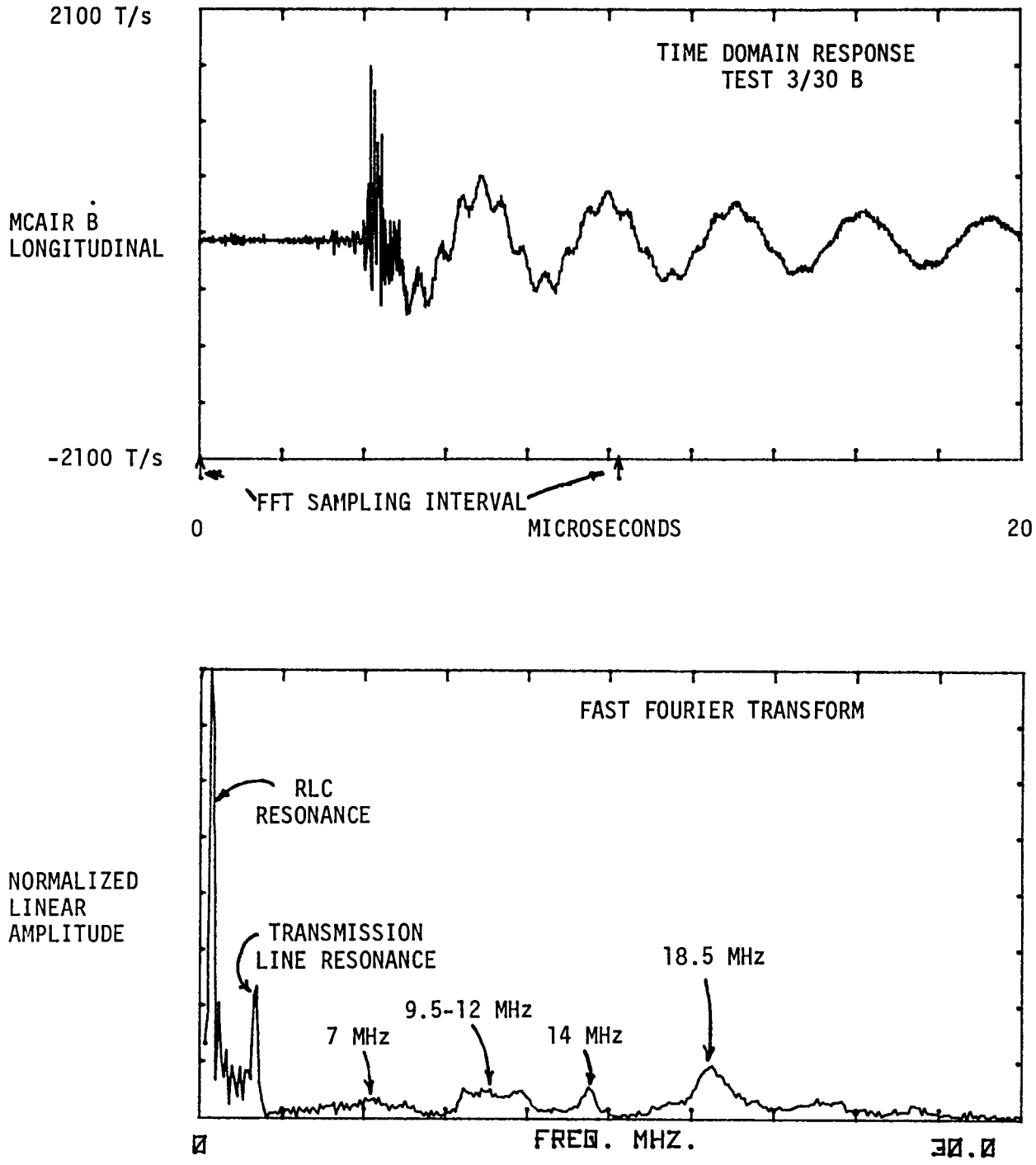

FIGURE 17 - MCAIR LONGITUDINAL $\dot{B}$ SENSOR RESPONSE AND 1024 DATA POINT FFT
(NO ADDED INDUCTANCE, HARD-WIRED AT TAIL HOOK)

FIGURE 17

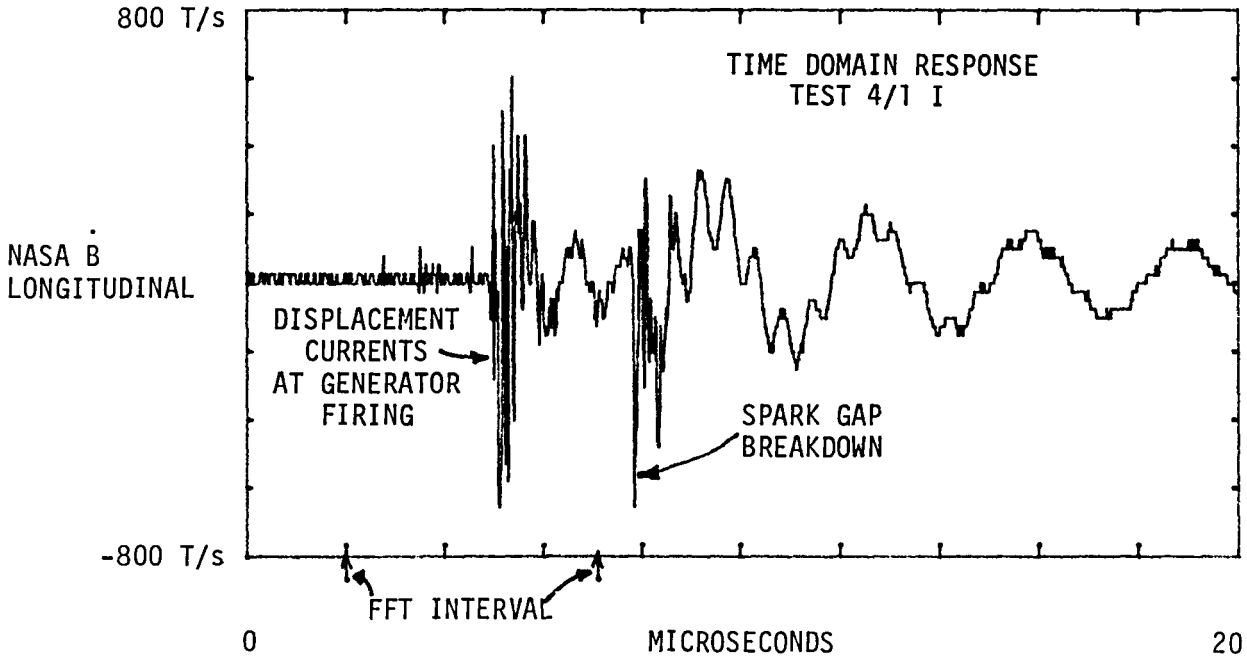

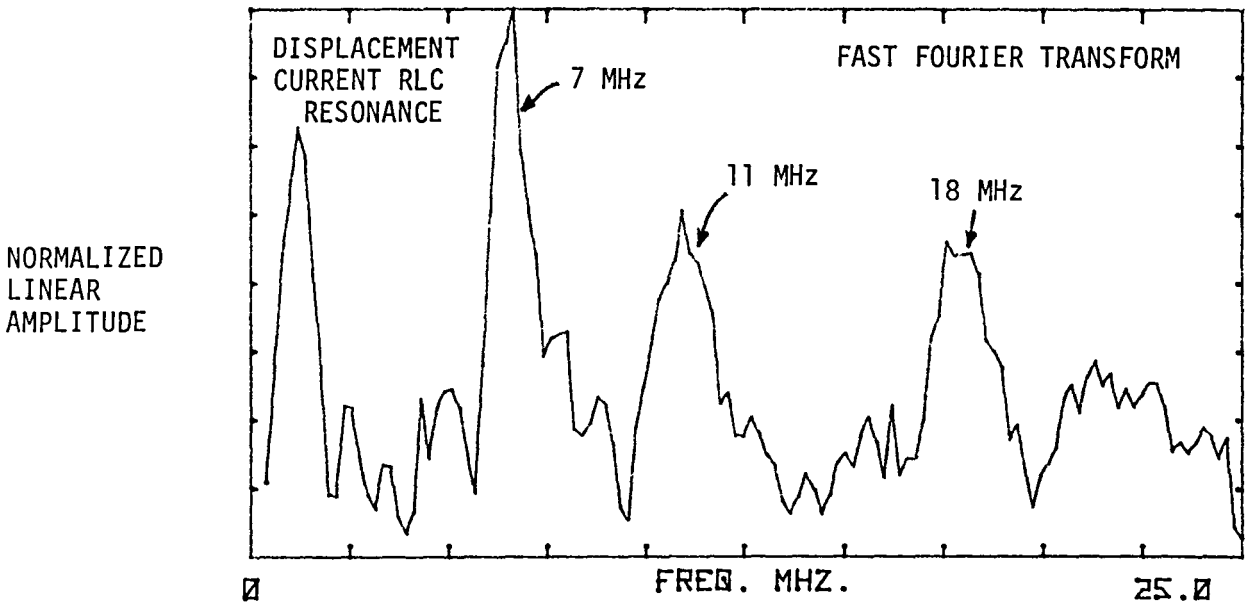

FIGURE 18 - NASA LONGITUDINAL B SENSOR RESPONSE AND 256 DATA POINT FFT (NO ADDED INDUCTANCE, 10-INCH ARC FROM THE TAIL HOOK)

FIGURE 18

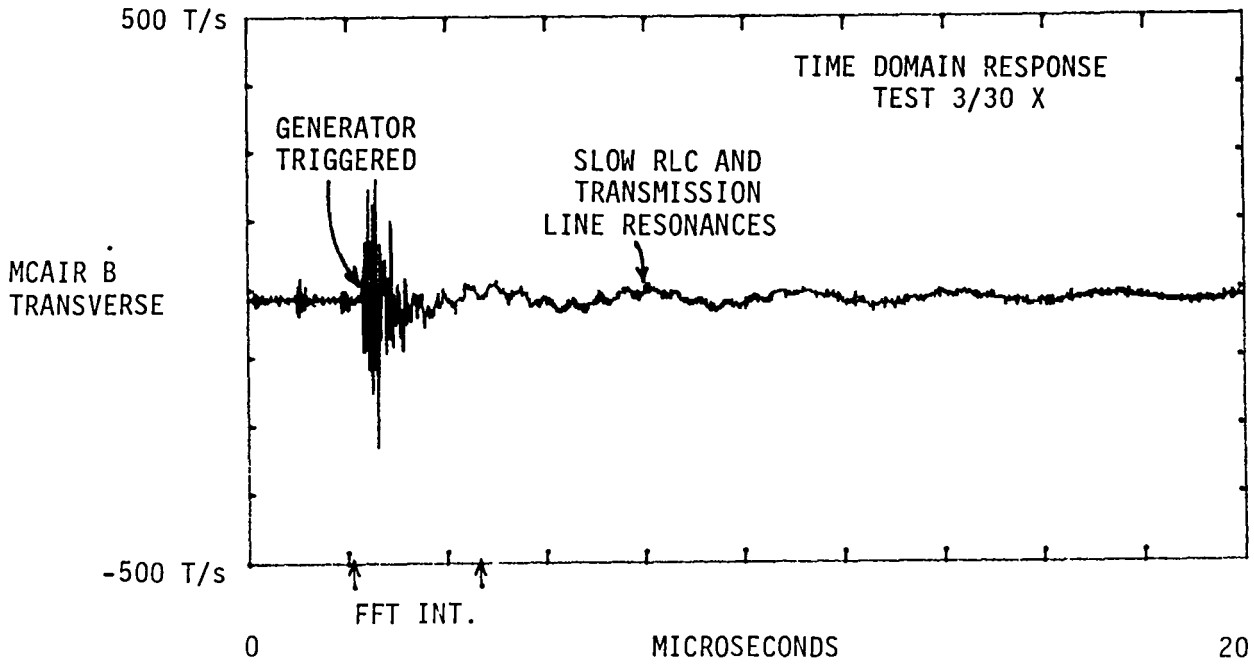

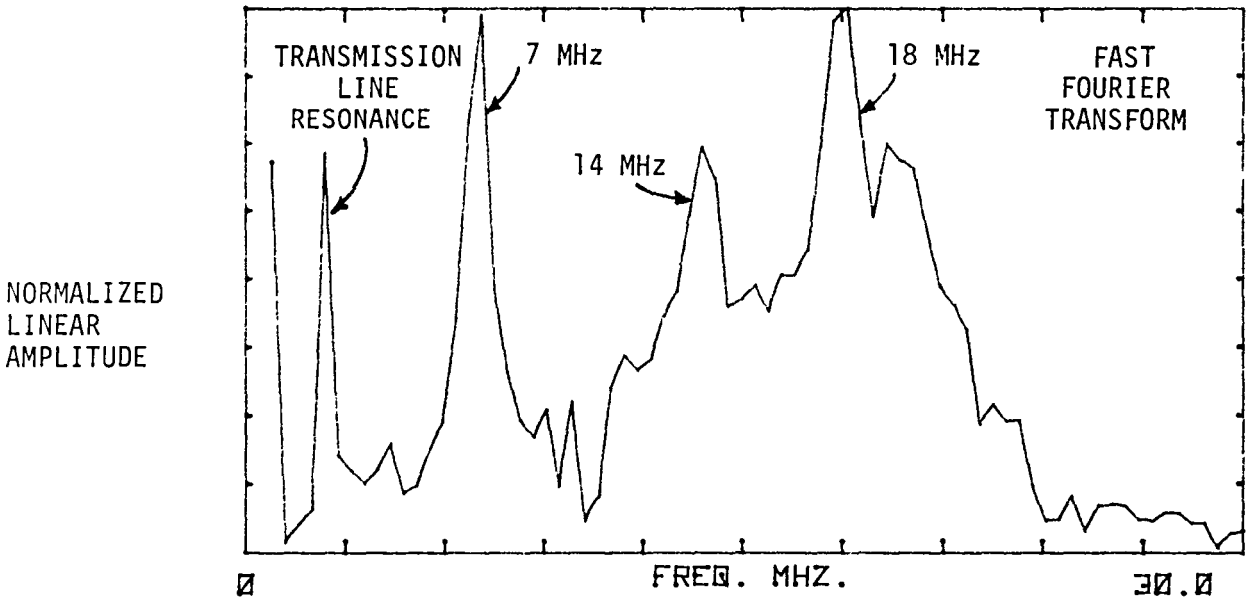

FIGURE 19 - MCAIR TRANSVERSE $\dot{B}$ SENSOR RESPONSE AND 256 DATA POINT FFT (NO ADDED INDUCTANCE, HARD-WIRED AT TAIL HOOK)

FIGURE 19

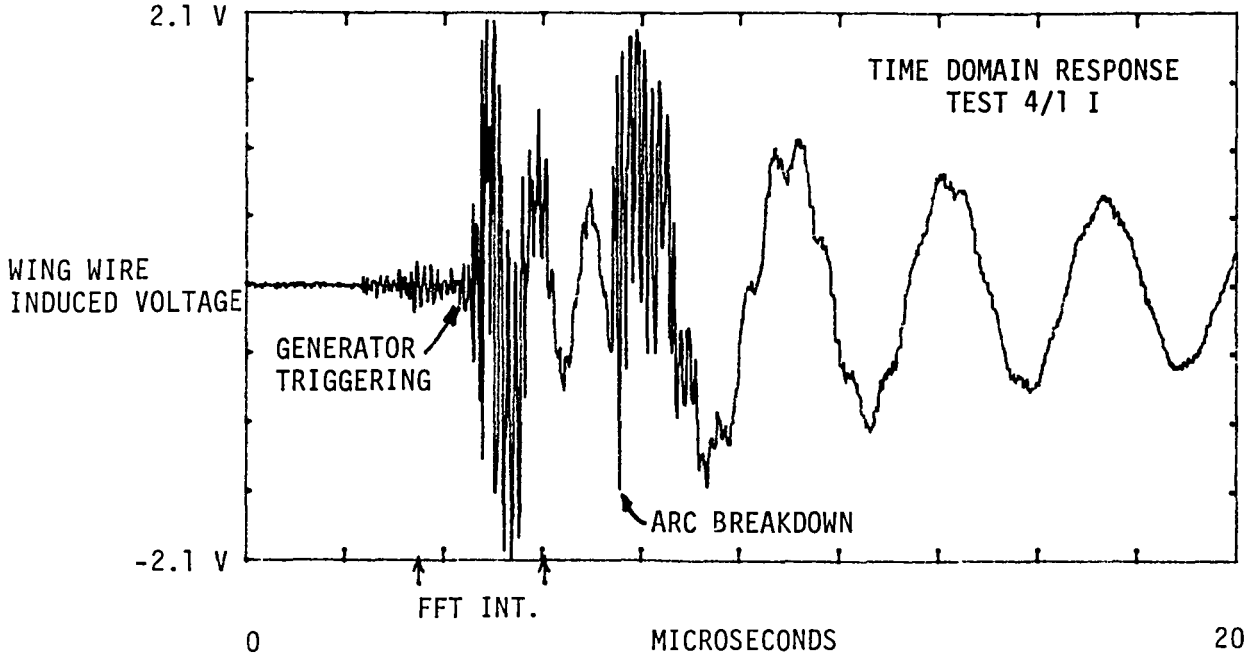

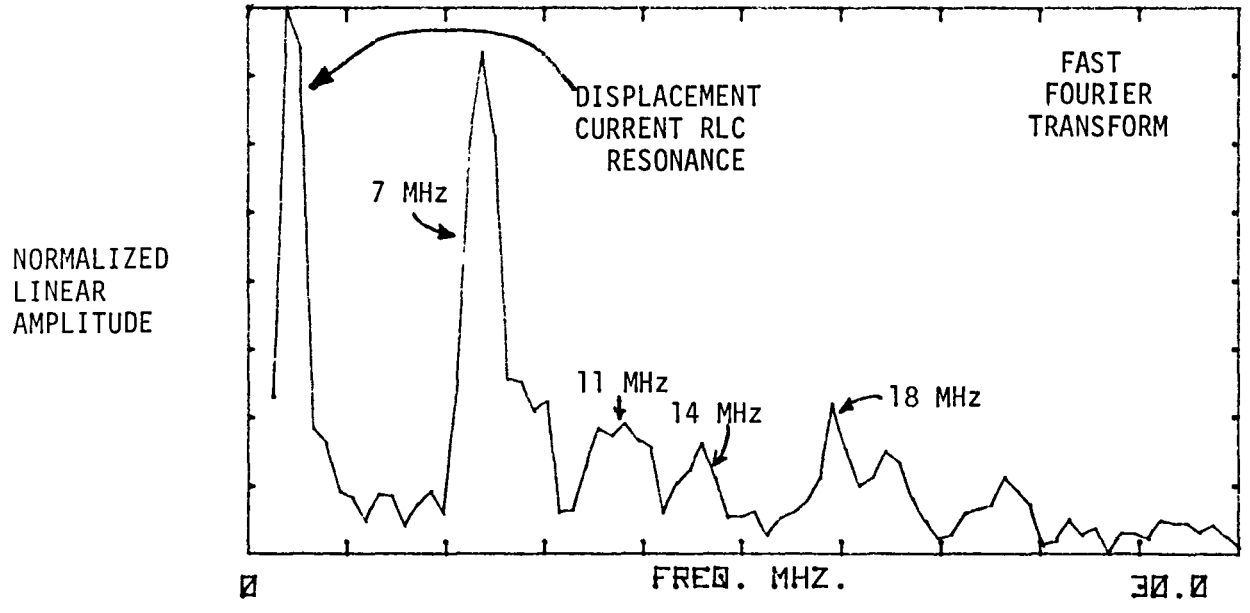

FIGURE 20 - WING WIRE INDUCED VOLTAGE RESPONSE AND 256 DATA POINT FFT (NO ADDED INDUCTANCE, 10-INCH ARC FROM THE TAIL HOOK)

FIGURE 20

6.0 RADIATED TEST RESULTS

The final day of testing was devoted to radiated tests using the terminated two-wire transmission line arrangement, described in Section 3.2. The purpose of the tests was to determine the characteristic aircraft resonances with the aircraft completely isolated from the stimulus source and ground potential. The only connections made to the aircraft were fiber optic data links from the screen room to the instrumentation bay. NASA $\dot{D}$ sensors on the aircraft and MCAIR field and current sensors were used to measure the system response. Tests were conducted without the engine running and with the bomb bay doors both open and closed. No other system configuration changes were made during the tests. Many redundant shots were conducted to measure all sensor and system parameters and to demonstrate data repeatability.

6.1 TIME DOMAIN DATA. For the radiated tests, the transmission line system was aligned so that the electric field between the two lines was parallel with the aircraft axis. Therefore, the incident electric field drove longitudinal displacement currents which oscillated at the aircraft's natural frequencies. The resulting aircraft voltage variations were monitored using the NASA $\dot{D}$ sensors. Figures 21 and 22 show the time domain responses of the $\dot{D}$ sensors, the incident electric field, and the current pulse in the transmission line.

The axial electric field component of the incident pulse was measured with a MCAIR spherical E-field sensor approximately 30 feet from and at the height of the right wing tip. The sensor is normally used to measure high electric fields and includes a large frequency compensated high-impedance attenuator. The radiated fields were of much lower amplitude than normally measured, so that the attenuated output had to be measured on a sensitive

TEST 4/2M

BOMB BAY DOOR CLOSED

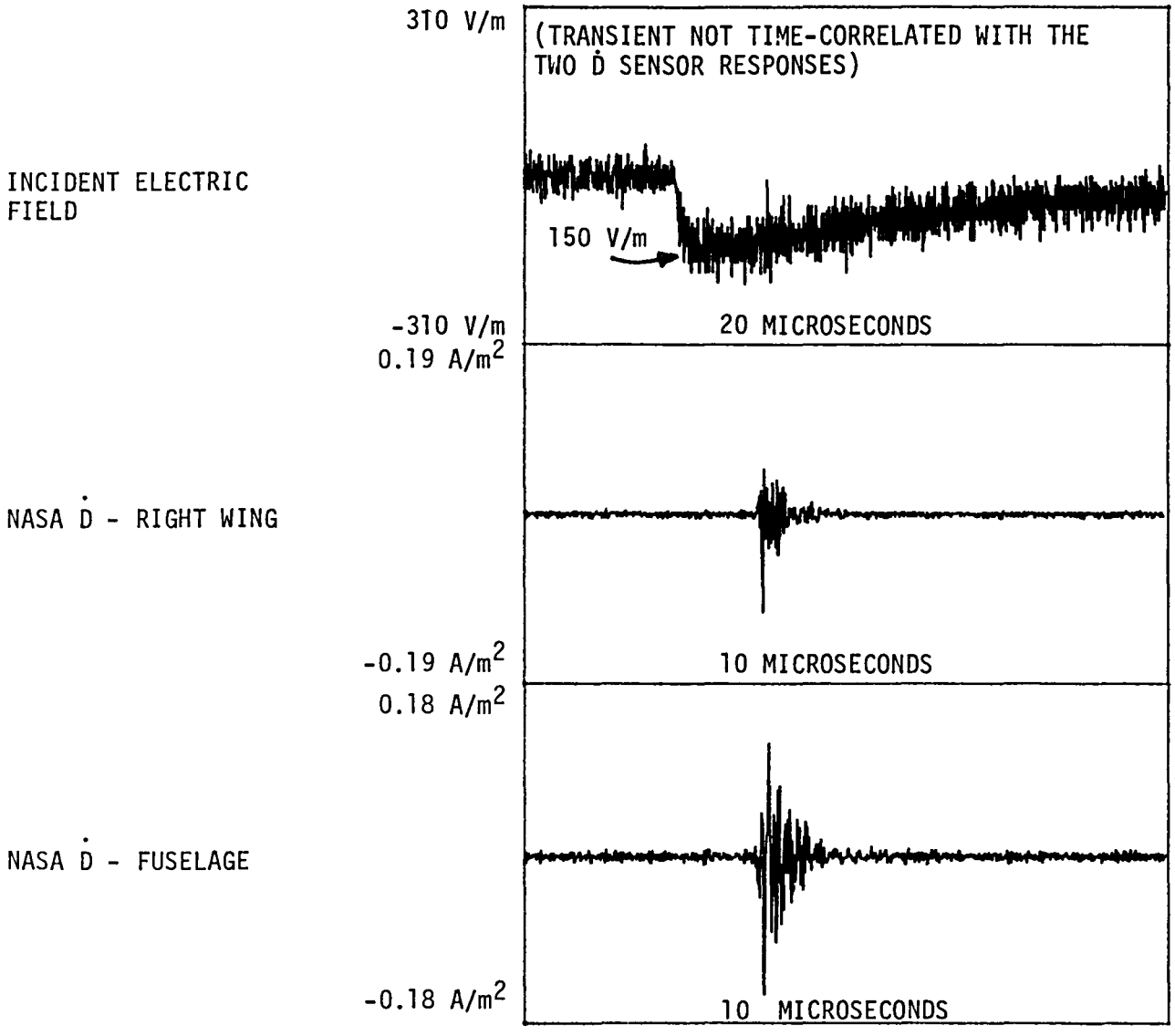

FIGURE 21 - TYPICAL RADIATED TEST TRANSIENTS; E-FIELD AND RIGHT WING AND FUSELAGE Ḋ SENSOR RESPONSES

FIGURE 21

TEST 4/2W

BOMB BAY DOOR CLOSED

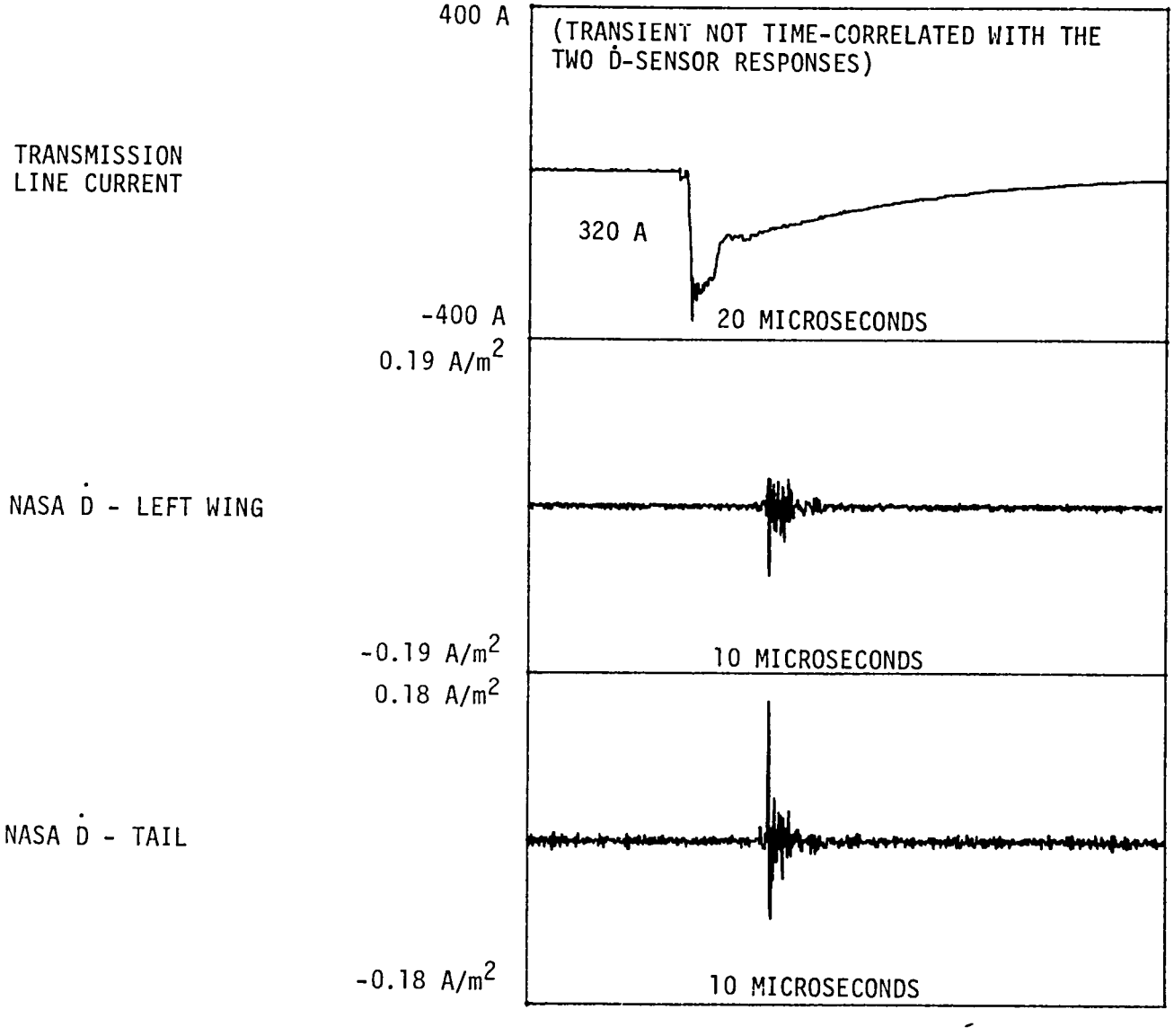

FIGURE 22 - TYPICAL RADIATED TEST TRANSIENTS; TRANSMISSION LINE CURRENT AND LEFT WING AND TAIL Ḋ SENSOR RESPONSES

FIGURE 22

Biomation scale. The signal-to-noise ratio for these measurement conditions was only three to one, so good definition of the input field was not obtained. The measured E-field had a peak of approximately 150 V/m and a rise time of 0.5 μs.

The pulse current was measured at the high voltage output of the Marx generator. The generator output voltage was approximately 270 kV, and the current amplitude was 320 A with a 0.12 μs rise time. The current pulse contains a small notch roughly 700 ns after the pulse start. This time is consistent with a reflected wave (down-and-back time) from the slightly mismatched termination of the 100-meter long line. Since the amplitude of the reflected wave was small, no attempt was made to perfectly match the impedance of the line.

The $\dot{D}$ sensor responses were high frequency transients lasting only a microsecond. The $\dot{D}$ responses were measured with the transient recorders fastest sampling interval of 5 ns to provide as much signal detail as possible. The amplitudes of the fuselage and tail responses were approximately 0.35 A/m^2 peak-to-peak and were about three times larger than the wing sensor responses. In general, the $\dot{D}$ transient responses were repeatable in waveshape and amplitude, and in the time domain it made very little difference whether the bomb bay doors were open or closed for this particular direction of the radiated pulse.

6.2 FREQUENCY DOMAIN DATA. Figures 23 through 26 show expanded time domain traces and the fast Fourier transforms of the $\dot{D}$ transients shown previously in Figures 21 and 22. The 256 sampling point routine was used to produce the FFT's. The FFT data are plotted on a normalized linear scale and are the transform of the derivative sensors outputs. To determine the

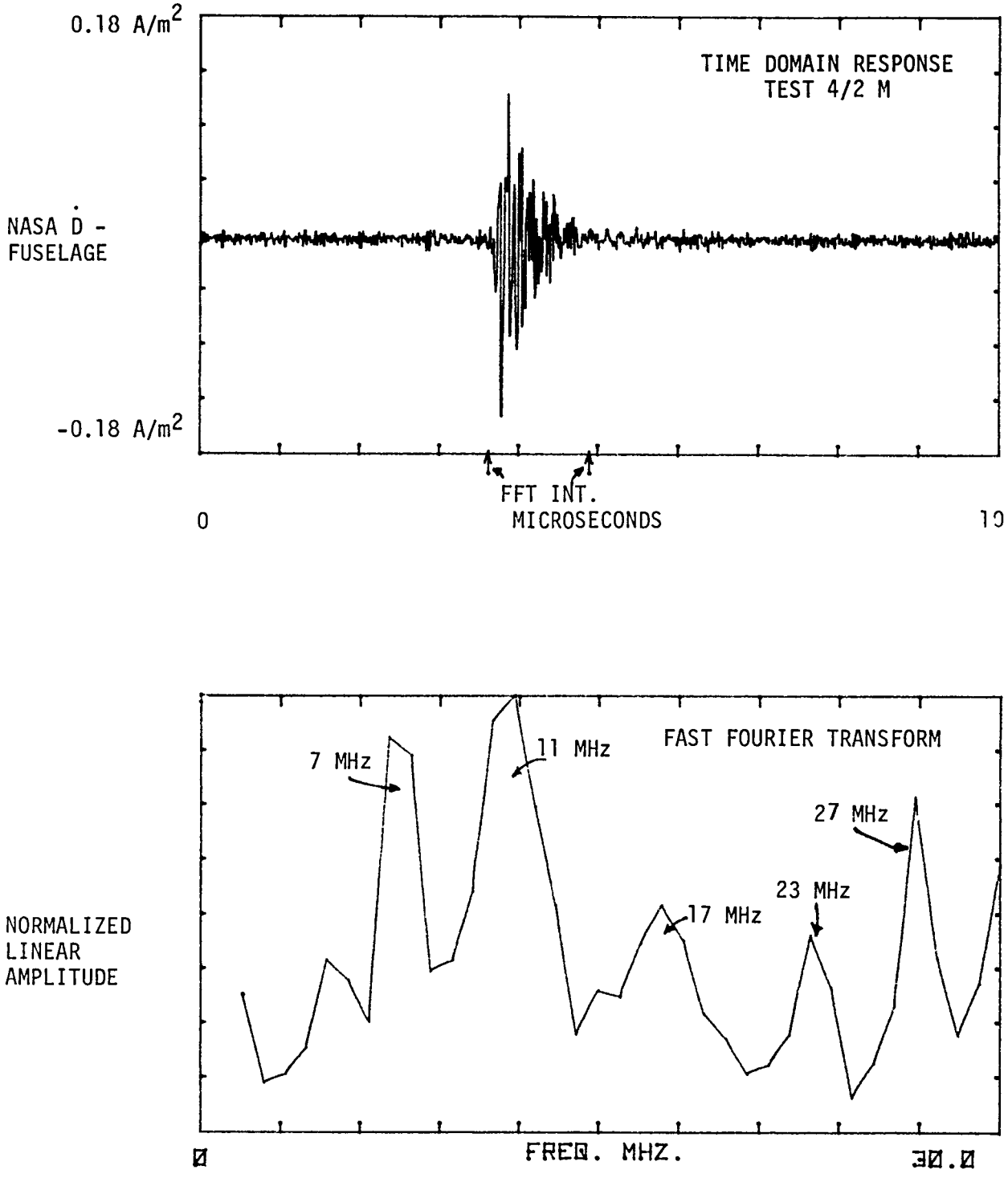

FIGURE 23 - FUSELAGE D SENSOR RESPONSE AND FFT FOR RADIATED TEST CONDITIONS

FIGURE 23

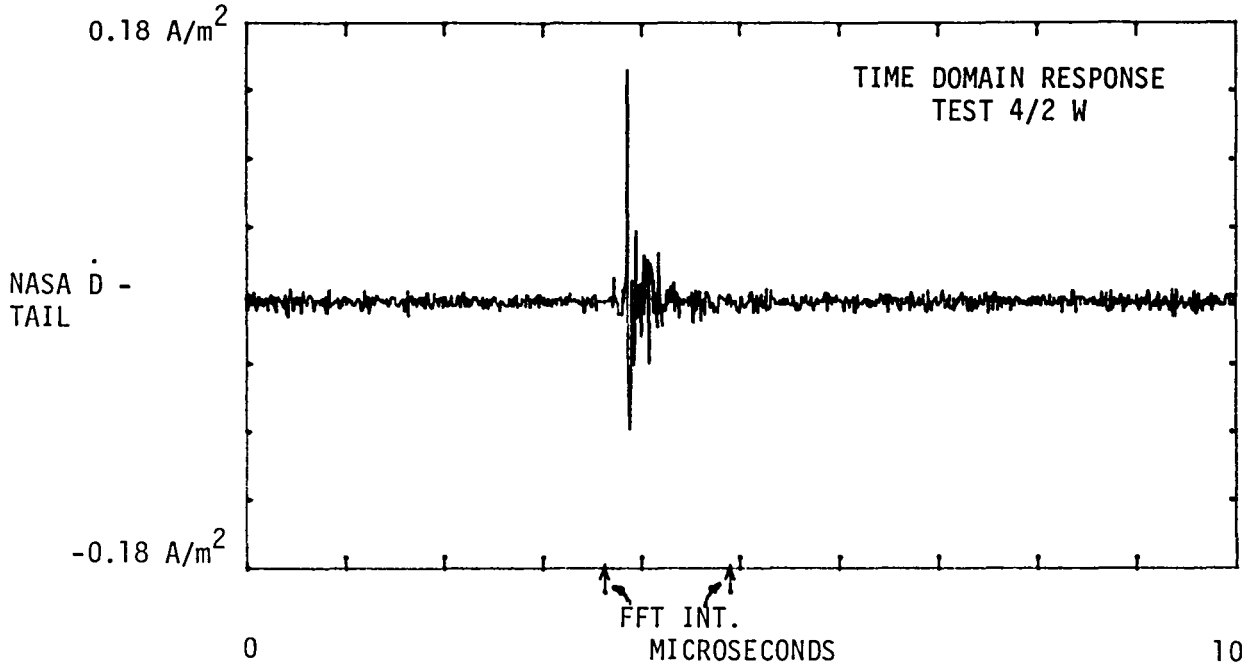

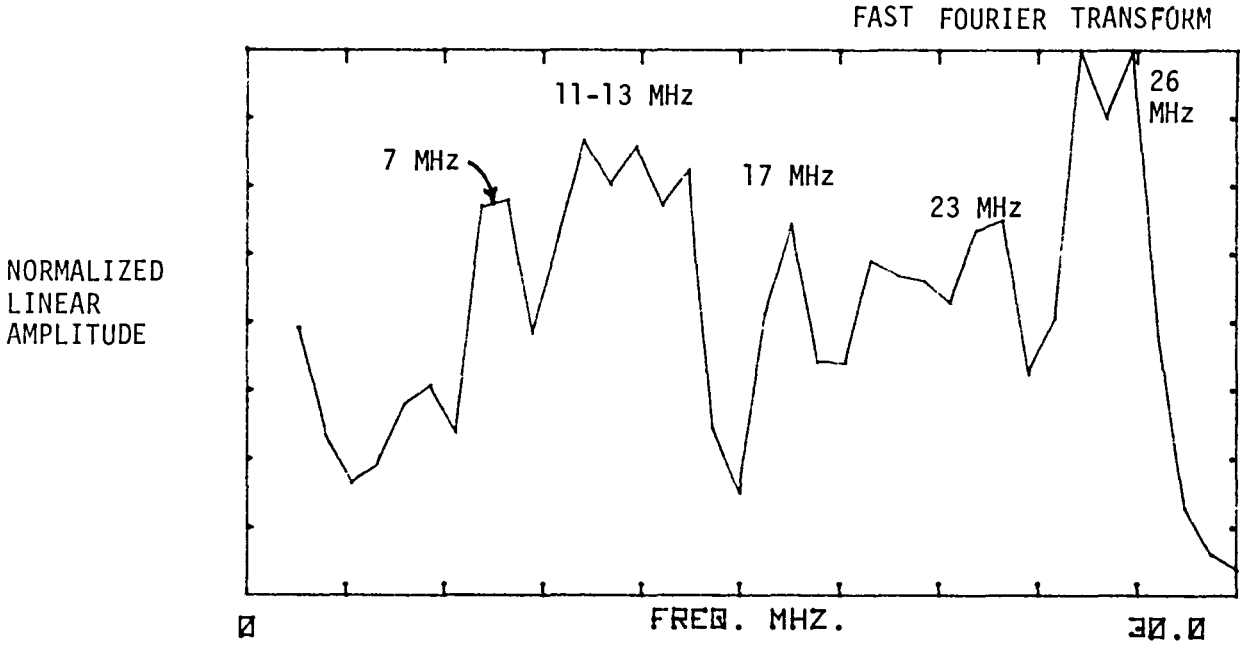

FIGURE 24 - TAIL D SENSOR RESPONSE AND FFT FOR RADIATED TEST CONDITIONS

FIGURE 24

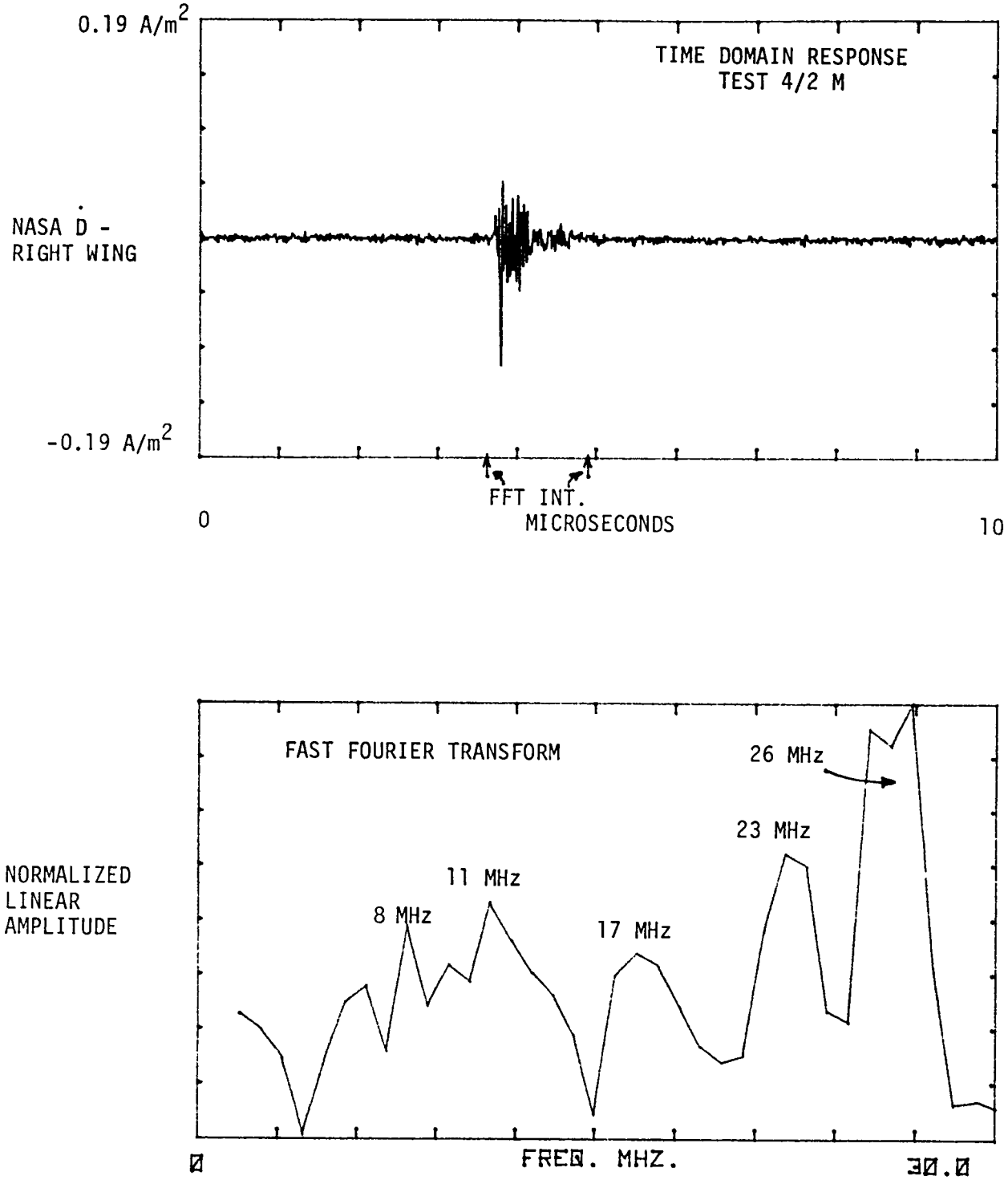

FIGURE 25 - RIGHT WING D SENSOR RESPONSE AND FFT FOR RADIATED TEST CONDITIONS

FIGURE 25

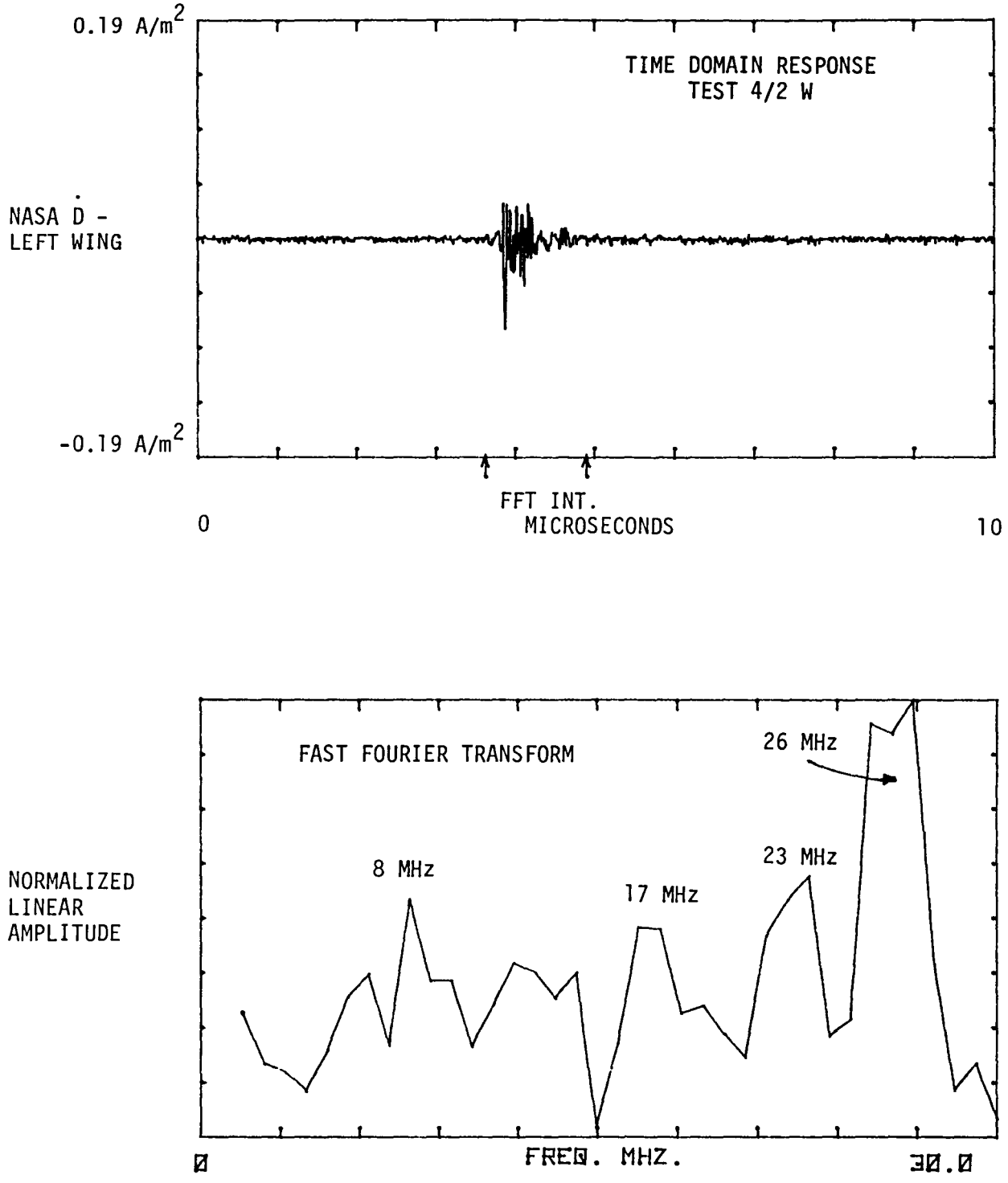

FIGURE 2 - LEFT WING D SENSOR RESPONSE AND FFT FOR RADIATED TEST CONDITIONS

FIGURE 26

relative spectral magnitudes of D (the electric displacement vector) from the $\dot{D}$ spectra, the plotted $\dot{D}$ spectra must be divided by $2\pi f$ where f is the frequency. In the resulting D transform, the amplitude of the higher frequency peaks will be reduced relative to the lower frequency peaks.

The radiated frequency domain traces generally show several high-frequency peaks. In most cases the peaks are well defined, but in others a band of frequencies several MHz wide is present. The frequency resolution of the 256 point FFT with the fast sampling rate is only ≈0.8 MHz so the peaks are only approximately located. The primary resonances generally occur at frequencies of 7, 11, 17, 23, and 26 MHz. The 7-, 11-, and 17-MHz oscillations were also observed in the direct attachment tests. The 14 MHz seen in the transverse sensors of the direct attachment case is not present in the radiated data since the excitation was primarily longitudinal. The higher harmonics at 23 and 26 MHz observed in the radiated tests were masked by the more dominant lower frequencies in the direct attachment tests.

7.0 CONCLUSION

The MCAIR lightning simulation ground tests accomplished all program objectives. All NASA sensors and interior wires were monitored for a wide variety of test conditions, and their responses were compared to externally-mounted MCAIR sensors. The sensor responses were repeatable, self-consistent, and in general agreement with values predicted in pretest calculations. The interior wire responses were inductively coupled to the aircraft currents and produced sizeable induced voltages during both the displacement current (charging) and discharge phases of the shock-excitation tests.

The direct attachment tests produced three types of frequency resonances. The overall system RLC response was dependent on the bulk system parameters and agreed well with values predicted from simple RLC circuit theory. A strong transmission line resonance at ≈2 MHz was present in most data and was due to the physical arrangement of the test setup and the terminations at the ends of the aircraft/return conductor transmission line. Aircraft resonances, due to the geometry of the F-106B itself, were also measured, but were somewhat masked by the transmission line and RLC resonances. In the direct attachment tests, aircraft frequencies of approximately 7, 11, 14, and 18 MHz were measured. In the radiated tests, aircraft resonances were measured at approximately 7, 11, 18, 23 and 26 MHz. These measured aircraft frequencies generally agree with the observed resonances in the flight data at 7, 8, 13 and 21 MHz and with scale model test resonances at 8, 14, 16, 19 and 24 MHz as described in Reference 1.

APPENDIX A

PRINCIPAL MCAIR TEST EQUIPMENT

Inclusive pages: 61-70

1. HIGH-VOLTAGE GENERATOR SYSTEM. The high-voltage generator system was specifically designed for remote site testing. The high-voltage Marx generator is modular in construction. Its output voltage is readily varied from 50 kV to 1.5 MV by changing the number of stages. The generator charging system is pneumatically controlled for isolation and is fail-safe in it operation.

Figure A-1 is a schematic of the system which includes the high-voltage Marx generator, a power supply, and an oil-filled charge/dump system. The generator, shown in Figure A-2, is built in modules with each shelf being an interchangeable generator stage. Up to 15 stages can quickly be assembled using only the shelves and dielectric supports for mechanical strength. Each shelf contains the capacitor, three resistors, spark gap switch, trigger electrode, and a grading ring. Each capacitor stage is rated at .032 μf and 100 kV. Interchangeable 40 KΩ copper sulfate resistors interconnect the capacitor terminals and trigger electrodes from one stage to the next. Each stage is triggered with an electrode biased at approximately half the potential between the copper-sphere spark gap electrodes. A grading ring is used on each shelf to suppress corona and produce a smoother electric field distribution.

Control of the generator system is provided by a pneumatically-operated charge/dump switch which totally isolates the generator from ground during firing. This system minimizes ground loops and coupling to the power supply and provides excellent operator safety. To charge the generator, the operator must depress a spring-loaded valve to apply air pressure to a pneumatic actuator which connects the power supply to the generator. When the valve is released, the following sequence quickly occurs: 1) the power supply and its ground are disconnected from the generator, 2) a trigger signal is applied to the trigger circuit, 3) the generator erects to high voltage, and 4) both sides of the

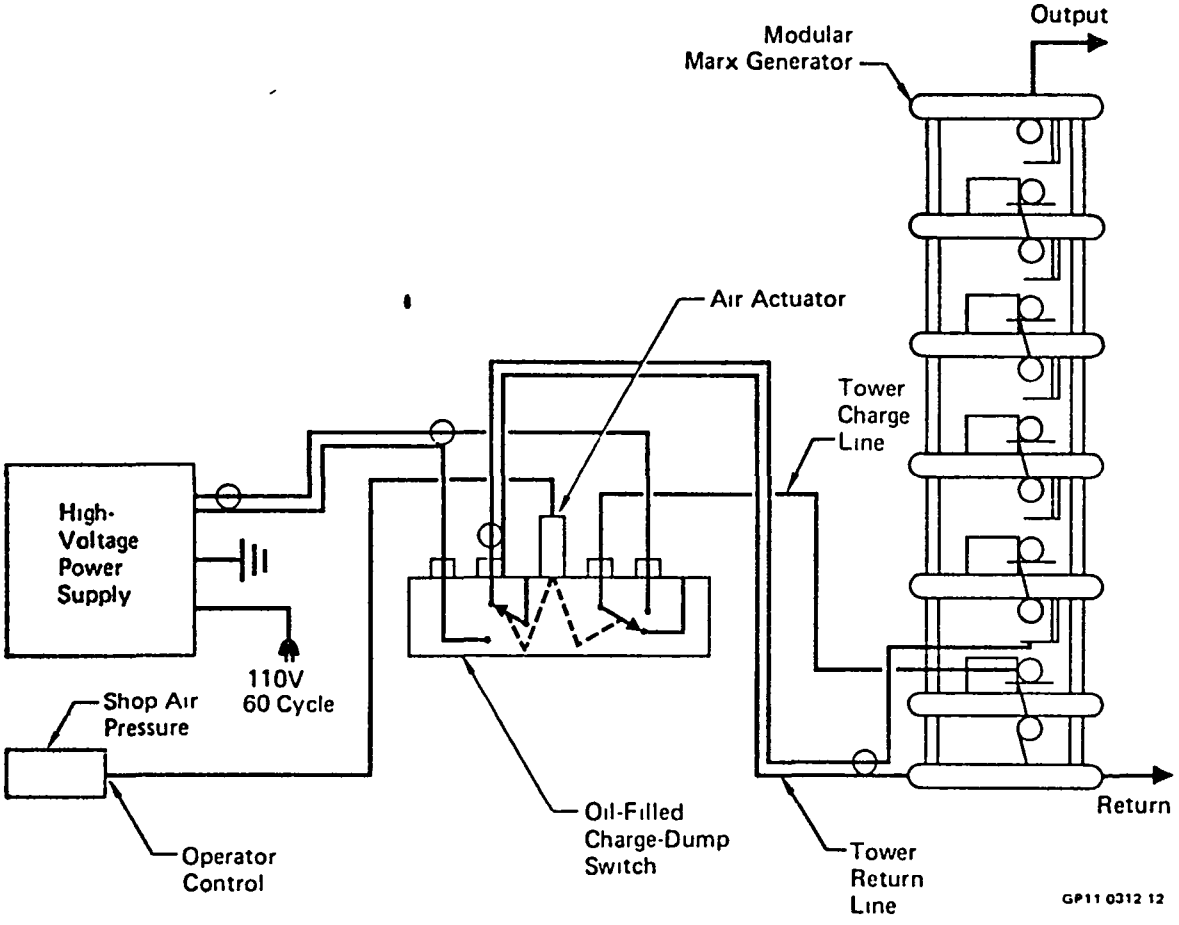

FIGURE A-1. HIGH-VOLTAGE GENERATOR SYSTEM DIAGRAM

FIGURE A-1

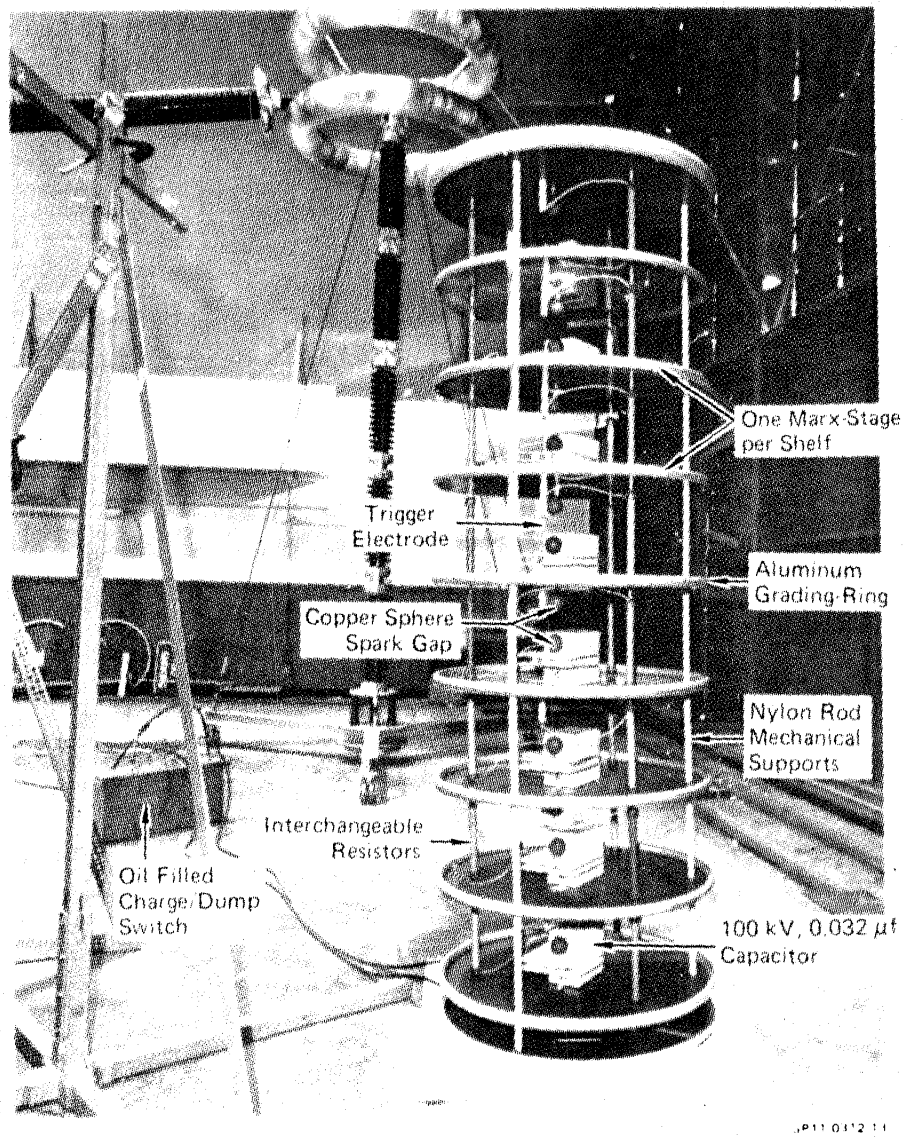

FIGURE A-2. MODULAR HIGH-VOLTAGE GENERATOR

FIGURE A-2

capacitor string are connected to ground. If for some reason the generator does not fire at step 3, the sequence continues and in step 4 the generator is discharged to ground through the charge/dump relay system.

2. FIBER OPTIC SYSTEM. The fiber optic data links, pictured in Figure A-3, were designed and constructed at MCAIR. These units were used in all tests to transmit the electrical response measured at the sensor to the recording equipment located in an RFI tight screen room. The use of fiber optics eliminates common mode interference and ground loop problems caused by the severe electromagnetic test environment.

The MDC fiber optic transmitter uses a high impedance differential amplifier to drive a current amplifier which in turn drives the light-emitting diode within its linear range. The output is a signal modulated light pulse which is transmitted through 20 meters of multistranded fiber optic cable to the receiver located in the screen room. The transmitter has common mode rejection of ≈40 dB at 15 MHz and can produce variable voltage gains from one to ≈150. The transmitter is battery-powered with a usable charge life of ≈4 hours. It can, therefore, be utilized anywhere in the test environment without external power and common mode signal problems. The dielectric fiber optic cable provides excellent high-voltage isolation.

The fiber optic receiver reconverts the optical signal into its electrical equivalent. The main receiver components are the receiver diode, a video amplifier, and a current amplifier to drive the 50Ω input impedance of the transient recorders. The entire fiber optic system has undergone several modifications during its development to improve reliability and bandwidth. The current system has a bandwidth of 25 MHz.

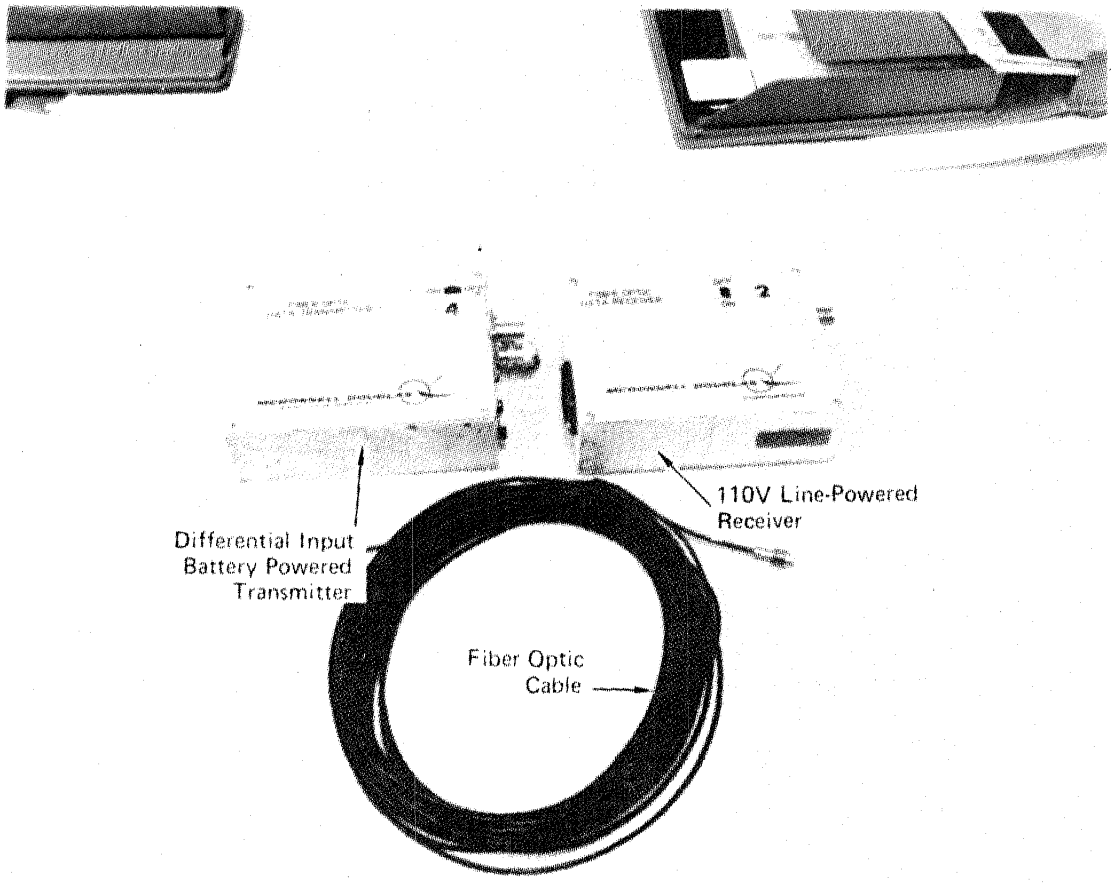

FIGURE A-3. FIBER OPTICS COMPONENTS

FIGURE A-3

3. DATA RECORDING AND REDUCTION. The data recording system, shown schematically in Figure A-4 and photographically in Figure A-5, is housed in a shielded enclosure for testing. The main components include four transient recorders (two Biomation 6500's, one Biomation 8100, and one Tektronix 7612D) and a Hewlett-Packard 9825 microcomputer with additional plotter and floppy-disk capability.

The transient recorders are operated in their "pretrigger" mode so that the baseline and leading edge of the transient response can be recorded. The 8100 samples 2,048 data points with nominal 8-bit resolution at a sampling rate of one datum point every ten nanoseconds. The 6500's have 6-bit resolution and sample every 20 nanoseconds for a total of 1,024 data points. The Tektronix 7612D has 8-bit resolution, 2,048 data points, and samples every ten nanoseconds for most test applications. All four recorders are triggered from the Biomation 8100 and can be time correlated to better than 50 nanoseconds.

The entire data acquisition system is controlled by the HP 9825 with software developed for transient analysis testing. The software is structured so that one controlling program is used to call any of 28 subroutines to perform the basic data recording, display, storage, and processing tasks. Memory space is held to a minimum by having only the controlling program and a binary FFT program in memory at any time. Data are stored on magnetic tape to provide a permanent record.

4. DATA SYSTEM CALIBRATION. Prior to each test series, the total data system including the fiber optics, the transient recorder, and the computer is calibrated for bandwidth and linearity. To do this, a high-frequency triangular wave is applied at the fiber optic transmitter of each data channel. The wave is adjusted in amplitude up to a point that nonlinearity can be seen on the

(A fourth transient recorder and two additional fiber optic channels were used at times in the AV-8B wing tests.)

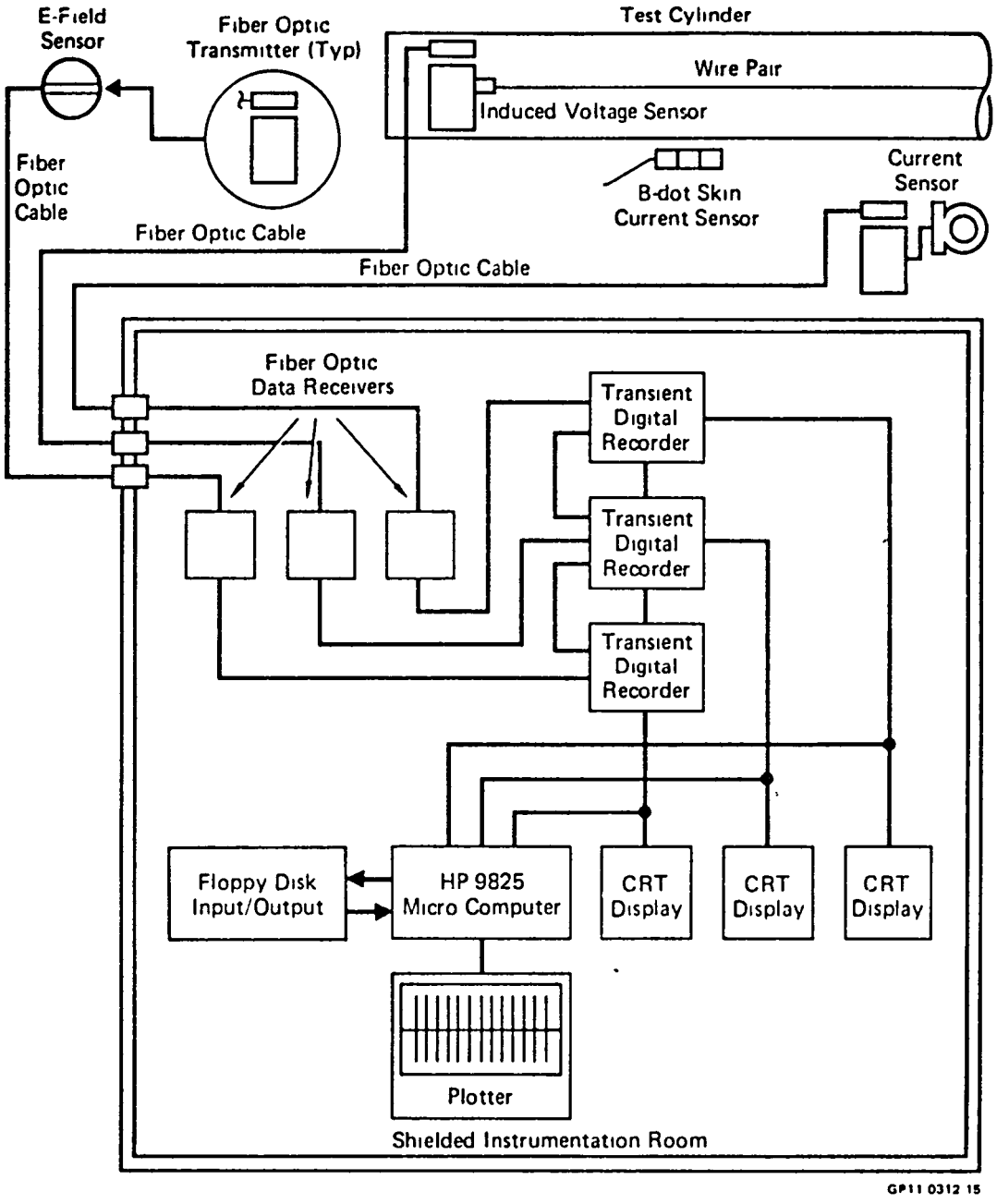

FIGURE A-4. INSTRUMENTATION SYSTEM FOR INDUCED COUPLING

FIGURE A-4

(A fourth transient recorder and two additional fiber optic channels were used in the F-105B tests.)

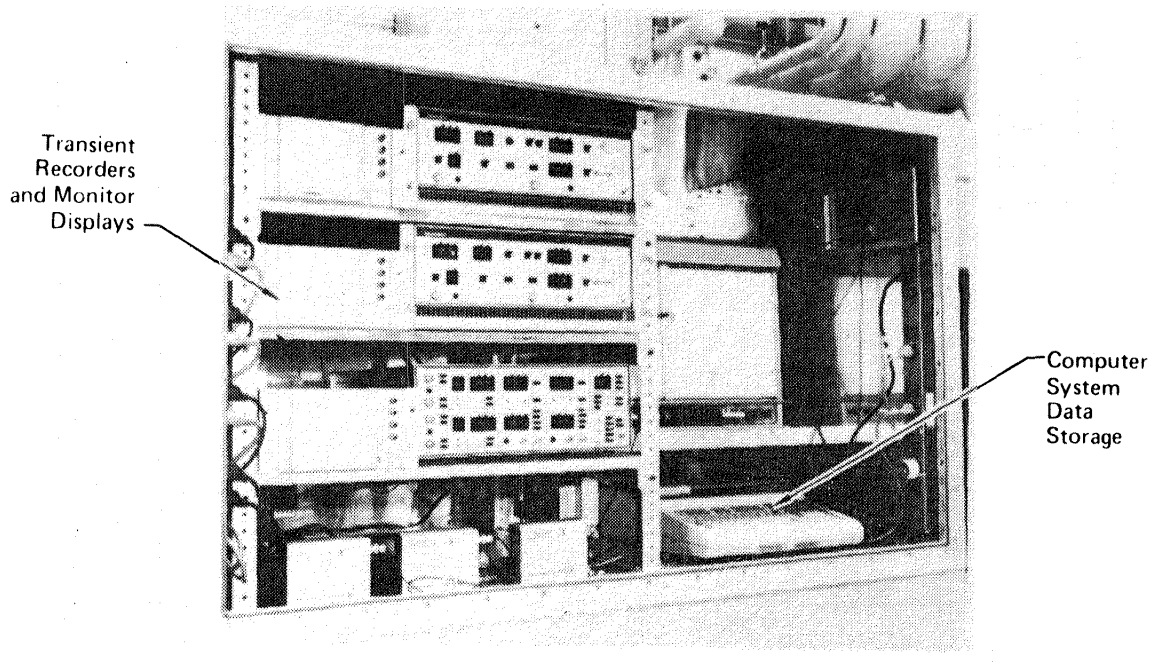

FIGURE A-5. ADVANCED PORTABLE DATA SYSTEM

FIGURE A-5

recorder's monitors. This known amplitude then establishes the maximum point at which data can be recorded and still maintain accuracy. The triangular calibration signal in the transient recorder memory is then loaded into the computer. This signal with its calibrated peak-to-peak voltage is used to establish all of the recorded signal levels.

5. DIELECTRIC ISOLATION SYSTEM FOR THE AIRCRAFT WHEELS. The lightning test article must be completely isolated from ground potential if it is to be charged to a high potential as required in the shock-excitation test technique. The isolation of a fighter aircraft whose landing gear hubs are less than 6 inches above ground is not a simple task. Surface tracking along a dielectric or arcing to ground potential from the wheels or other extremities near ground provide alternate current paths which greatly reduce shot-to-shot repeatability and complicate test understanding.

Figure A-6 is a schematic of the dielectric pads used to isolate the F-106B nose and landing gears. This pad design has evolved from our previous full-scale aircraft tests and easily withstood up to 320 kV applied during these tests. The 4-foot by 4-foot base of the pad prevented direct dielectric puncture and consisted of six sheets of 1/4-inch Lexan covered with two sheets of 1/4-inch polyvinyl chloride (PVC). The sidewalls prevented surface tracking along the dielectric and arcing around the base. The sidewall supports were two concentric rings of PVC strip that were plastic-welded to the base sheets. The sidewalls were continuous 12-inch-high strips of Lexan that were coiled to provide a thickness of 3/4 inch. A toroidal aluminum grading ring and a shallow depth of transformer oil between the vertical supports were used to prevent dielectric puncture at the weld seams.

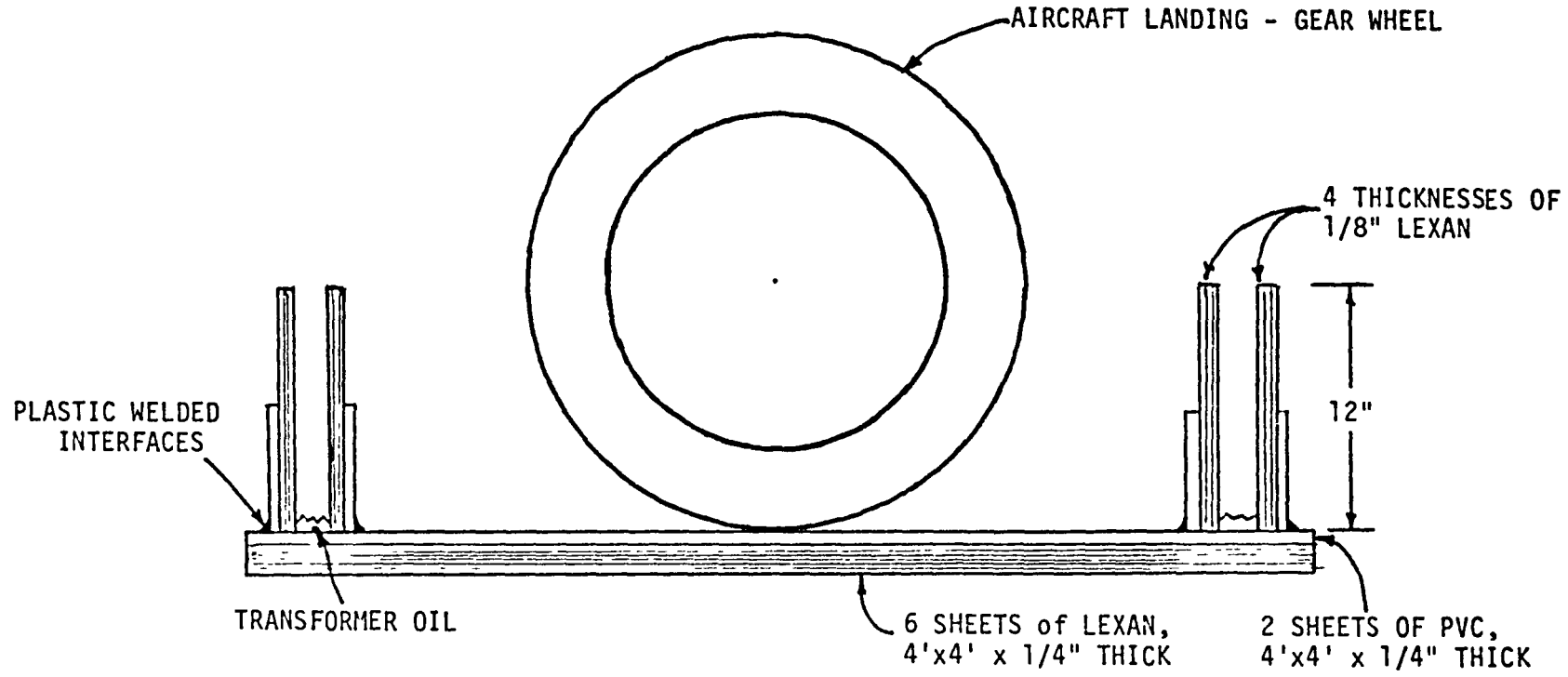

FIGURE A-6. DIELECTRIC ISOLATION PAD SCHEMATIC

APPENDIX B

TEST MATRIX

Inclusive pages: 72-76

SENSOR LEGEND AND ABBREVIATIONS
(USED WITH THE TEST MATRIX)

NASA SENSORS	SENSOR TYPE AND LOCATION	MDC SENSORS
B_{1N}	TRANSVERSE B-DOT SENSOR - FUSELAGE	B_{1M}
B_{2N}	LONGITUDINAL B-DOT SENSOR - FUSELAGE	B_{2M}
B_{3N}	B-DOT SENSOR - LEFT WING	B_{3M}
B_{4N}	B-DOT SENSOR - RIGHT WING	B_{4M}
	B-DOT SENSOR - LOWER FORWARD FUSELAGE	B_{5M}
D_{1N}	D-DOT SENSOR - LOWER FORWARD FUSELAGE	D_{1M}
D_{2N}	D-DOT SENSOR - VERTICAL STABILATOR	D_{2M}
D_{3N}	D-DOT SENSOR - LEFT WING	D_{3M}
D_{4N}	D-DOT SENSOR - RIGHT WING	D_{4M}
	E-FIELD SENSOR	E
	VOLTAGE DIVIDER	V
	CURRENT SENSOR	I
	I-DOT SENSOR	I_M
I_N	I-DOT SENSOR - NOSE	
I_{2N}	CURRENT SENSOR - NOSE	
I_{3N}	CURRENT SENSOR - FUSELAGE WIRE	

ABBREVIATIONS

L	INDUCTANCE (μH)
HW	HARD-WIRED
F/O	FIBER OPTICS
FW	FUSELAGE WIRE
WW	WING WIRE
RW	RIGHT WING
LW	LEFT WING
NC	NOT CALIBRATED
RAD	RADIATED
BG	BACKGROUND
GEN	GENERATOR
GO	GENERATOR OUTPUT

SHOT NO.	TRK-FILE	ADDED L(μH)	OUTPUT	CH 1	CH 2	CH 3	CH 4	CH 5	COMMENTS
INPUT INDUCTANCE MEASUREMENT									
3/29CAL	0-0	F/O CALIBRATION							
3/29A	0-1	0	HW-GEN	-	-	(I-BOOM, 1000X	-	-	MEASURE L
3/29B	0-2	0	"	-	-		-	-	
HARD-WIRED TESTS TO DETERMINE APPROPRIATE SENSOR LEVELS: BOMB BAY OPEN AND THE AIRCRAFT UNPOWERED									
3/29C	-	0	HW-TAIL	D_{2N}-32 dB	D_{4N}-20 dB	"	D_{1N}-36 dB	D_{3N}-32 dB	
3/29D	0-3	0	"	"	"	"	"	"	
3/29E	0-4	0	"	"	"	"	"	"	
3/29F	0-5	0	"	"	-	100X	"	"	F/O CHANGE-CH 3
3/29G	0-6	0	"	BG	BG	1000X	BG	BG	F/O CHANGE-CH 3
3/29H	0-7	0	"	B_{2N}-20 dB	B_{1N}-20 dB	"	B_{3N}-20 dB	B_{4N}-0 dB	
3/29I	0-8	0	"	"	"	"	B_{3N}-26 dB	B_{4N}-26 dB	
3/29J	0-9	0	"	"	"	"	"	"	
3/29K	-	0	"	"	"	"	"	"	
3/29L	0-10	0	"	I_{2N}-52 dB	I_N-38 dB	"	FW-43 dB	WW-43 dB	
3/29M	0-11	0	"	"	"	"	"	"	
WITH THE AIRCRAFT POWERED, COMPARED MDC AND NASA $\dot{B}$ SENSOR RESPONSES AT DIFFERENT SYSTEM INDUCTANCE LEVELS, HARD-WIRED OUTPUT FROM THE TAIL HOOK									
3/29N	0-12	0	"	B_{3N}-26 dB	B_{1M}-1X	"	B_{1N}-18 dB	B_{3M}-1X	CH 4 F/O DAMAGED
3/29O	0-13	0	"	"	"	"	"	B_{3M}-2X	"
3/29P	0-14	50	"	"	"	"	"	"	"
3/29Q	1-0	50	"	"	"	"	"	"	"
3/29R	1-1	200	"	B_{3N}-14 dB	B_{1M}-.5X	500X	"	"	"
3/29S	1-2	200	"	"	"	"	"	"	"
3/29T	1-3	200	"	B_{4N}-20 dB	B_{2M}-1X	"	B_{2N}-18 dB	B_{4M}-2X	"
3/29U	1-4	50	"	B_{4N}-26 dB	"	"	"	"	F/O CH 4, BATTERIES CH 5
3/29V	1-5	0	"	"	"	"	"	"	
3/29CHK	1-6	F/O BATTERY CHECK							
COMPARED INTERIOR WIRE, $\dot{B}_{2M}$, and $\dot{B}_{4M}$ FOR DIFFERENT HARD-WIRED OUTPUT LOCATIONS									
3/30CAL	1-7	F/O CALIBRATION							
3/30A	-	0	HW-TAIL	FW-42 dB	WW-42 dB	I-BOOM	B_{4M}-5X	B_{2M}-2X	
3/30B	1-8	0	"	FW-27 dB	WW-27 dB	1000X	B_{4M}-4X	"	WW-POOR GND
3/30C	1-9	0	"	"	"	"	"	"	WW & FW-POOR GND
3/30D	1-10	50	"	"	"	"	"	"	"
3/30E	1-11	0	HW-RW	"	"	"	"	"	FW-POOR GND
3/30F	1-12	0	"	"	"	"	"	"	FW & WW-POOR GND
3/30G	1-13	50	"	"	"	"	"	"	"
3/30H	1-14	0	HW-LW	"	WW-21 dB	"	B_{3M}-4X	"	"
3/30I	0-0	0	"	"	"	"	"	"	"
3/30J	0-1	50	"	"	"	"	"	"	"
3/30K	0-2	0	"	"	"	"	B_{5M}-4X	"	FW-POOR GND

SHOT NO.	TRK-FILE	ADDED L(μH)	OUTPUT	CH 1	CH 2	CH 3	CH 4	CH 5	COMMENTS
3/30L	0-3	0	HW-LW	FW-27 dB	WW-21 dB	I-BOOM	B_{5M}-4X	B_{2M}-2X	-
3/30M	0-4	0	"	"	"	1000X	"	"	
3/30N	0-5	50	"	"	"	"	"	"	
3/30O	0-6	0	"	BG	BG	"	"	"	
3/30P	0-7	0	"	"	"	"	"	"	
MONITORED $\dot{B}_{5M}$ AND THE FUSELAGE WIRE VOLTAGE AND CURRENT FOR LEFT WING TIP AND TAIL OUTPUT LOCATIONS									
3/30Q	0-8	0	"	FW-27 dB	-	"	"	B_{1M}-2X	
3/30R	0-9	0	"	"	-	"	"	"	
3/30S	0-10	50	"	"	-	"	"	"	
3/30T	0-11	0	"	I_{3N}-6 dB	-	"	"	"	
3/30U	0-12	0	"	"	-	"	"	"	
3/30V	0-13	0	HW-TAIL	"	-	I-TAIL	"	"	
3/30W	0-14	0	"	"	-	1000X	"	B_{1M}-1X	
3/30X	1-0	0	"	FW-27 dB	-	"	"	"	
3/30Y	1-1	0	"	"	-	"	"	"	
3/30Z	1-2	0	"	WW-21 dB	-	"	"	"	CH 1-NC
COMPARED MDC AND NASA $\dot{D}_1$ AND $\dot{D}_2$ SENSORS FOR SEVERAL ARC LENGTHS AND A TAIL OUTPUT. AIRCRAFT VOLTAGE WAS MONITORED IN SOME CASES									
3/30AA	1-3	0	"	D_{1N}-36 dB	-	"	D_{1M}-1X	D_{2M}-1X	
3/30BB	1-4	0	"	"	-	"	"	D_{2M}-5X	
3/30CC	1-5	0	"	D_{2N}-26 dB	-	"	"	"	CH 1-NC
3/30DD	1-6	0	4" ARC-TAIL	"	-	"	D_{1M}-2X	D_{2M}-10X	
3/30EE	1-7	0	"	D_{1N}-36 dB	-	"	"	"	
3/30FF	1-8	0	8" ARC-TAIL	"	-	"	"	"	CH 4, 5 BATTERIES
3/30GG	1-9	0	"	"	-	"	"	"	"
3/30CL2	1-10	F/O RECALIBRATION AFTER REPLACING BATTERIES IN CH's 4 AND 5							
3/30HH	1-11	0	8" ARC-TAIL	D_{1N}-36 dB	-	"	D_{1M}-2X	D_{2M}-10X	
3/30II	1-12	0	"	D_{2N}-26 dB	-	"	"	"	CH 1-NC
3/30JJ	1-13	0	10" ARC-TAIL	"	-	V-TAIL	"	"	"
3/30KK	1-14	0	"	"	-	2500X	"	"	"
3/30LL	0-0	50	"	"	-	"	"	"	"
3/30MM	0-1	0	"	D_{1N}-36 dB	-	"	"	"	
3/30CHK	0-2	F/O BATTERY CHECK							
COMPARED MDC AND NASA $\dot{D}$ SENSORS FOR AN OUTPUT SPARK GAP OF TEN INCHES FROM BOTH THE TAIL AND LEFT WING TIP LOCATIONS									
3/31CAL	0-3	F/O CALIBRATION FOR CH's 1, 3, 4, 5							
3/31CH2	0-4	SCALING WAVEFORM FOR UNCALIBRATED F/O CHANNEL							
3/31A	0-5	0	10" ARC-TAIL	D_{1M}-2X	-	I-TAIL	D_{1N}-36 dB	D_{2N}-26 dB	CH 1-NC, BATTERIES CH 4
3/31B	0-6	0	"	"	-	1000X	"	"	"
3/31C	0-7	0	"	"	-	"	"	"	"
3/31D	0-8	50	"	"	-	"	"	"	"
3/31E	-	50	10" ARC-LW	"	-	I-LW	"	"	NO PLOTTED DATA
3/31F	0-9	50	"	"	-	1000X	"	"	CH 1-NC, BATTERIES CH 4
3/31G	0-10	50	"	D_{2M}-10X	-	"	"	"	BATTERIES CH 4
3/31H	0-11	0	"	"	-	"	"	"	"
3/31I	0-12	0	"	D_{1M}-2X	-	"	"	"	CH 1-NC; BATTERIES CH 4
3/31J	0-13	50	10" ARC-LW	"	-	"	"	"	CH 1-NC; BATTERIES CH 4

SHOT NO.	TRK-FILE	ADDED L(μH)	OUTPUT	CH 1	CH 2	CH 3	CH 4	CH 5	COMMENTS
3/31CL2	0-14	REPLACED CH 4 F/O TRANSMITTER AND RECALIBRATED CH's 1, 3, 4, 5							
3/31K	1-0	0	10" ARC-LW	D_{3M}-2X	-	I-LW	D_{3N}-26 dB	D_{4N}-dB	CH 1-NC
3/31L	1-1	0	"	D_{4M}-10X	-	1000X	"	"	
3/31M	1-2	50	"	"	-	"	"	"	
3/31N	1-3	200	"	"	-	"	"	"	
3/31O	1-4	200	10" ARC-TAIL	"	-	I-TAIL	"	"	
3/31P	1-5	50	"	"	-	1000X	"	"	
3/31Q	1-6	0	"	"	-	"	"	"	CH 1-BATTERIES
3/31R	1-7	0	"	"	-	"	"	"	"
3/31S	1-8	0	"	D_{3M}-2X	-	"	FW-26 dB	WW-18 dB	WW-POOR GND; CH 1-BATTERIES-NC
3/31T	1-9	0	"	D_{4M}-10X	-	"	FW-29 dB	"	WW-POOR GND; CH 1-REPLACED BATTERIES
3/31U	1-10	0	"	D_{3M}-2X	-	"	"	"	WW-POOR GND; CH 1-NC
3/31V	1-11	0	"	E-250X	-	"	"	"	WW-POOR GND
3/31W	-	50	"	"	-	"	"	"	"
WITH A 10-INCH OUTPUT SPARK GAP AT THE TAIL, ALMOST ALL SENSORS AND WIRES WERE MONITORED FOR DIFFERENT SYSTEM INDUCTANCE LEVELS									
4/1CAL	1-12	CALIBRATION FOR F/O CH's 1, 3, 4, 5							
4/1CH1	1-13	SCALING WAVEFORM FOR UNCALIBRATED F/O CHANNEL							
4/1A	1-14	0	10" ARC-TAIL	I_{2N}-52 dB	-	"	WW-6 dB	FW-29 dB	CH 1-NC; CH 3-ARC TO GND
4/1B	0-0	0	"	B_{2N}-18 dB	-	"	"	"	CH 3-ARC TO GND
4/1C	0-1	0	"	"	-	"	"	"	"
4/1D	0-2	0	"	I_{2N}-52 dB	-	"	WW-12 dB	FW-35 dB	CH 1-NC; CH 3-ARC TO GND
4/1E	0-3	50	"	"	-	"	"	"	CH 1-NC
4/1F	0-4	50	"	"	-	"	"	"	"
4/1G	0-5	200	"	"	-	"	"	"	"
4/1H	0-6	0	"	"	-	"	"	"	"
4/1I	0-7	0	"	B_{2N}-18 dB	-	"	"	"	
4/1J	0-8	0	"	B_{1N}-18 dB	-	"	D_{2N}-21 dB	"	
4/1K	0-9	0	"	"	-	V-TAIL	"	"	
4/1L	0-10	50	"	"	-	2500X	"	"	
4/1M	0-11	200	"	"	-	"	"	"	
4/1N	0-12	0	"	WW-12 dB	-	"	"	"	CH1-NC
4/1O	0-13	50	"	"	-	I-TAIL	"	"	"
4/1P	0-14	200	"	"	-	1000X	"	"	"
4/1Q	1-0	200	"	B_{3N}-18 dB	-	"	B_{4N}-18 dB	D_{1N}-38 dB	"
4/1R	1-1	200	"	"	-	"	"	D_{1N}-44 dB	"
4/1S	1-2	50	"	"	-	"	"	"	"
4/1T	1-3	50	"	"	-	"	"	"	"
4/1U	1-4	0	"	"	-	"	"	"	"
4/1V	1-5	0	"	"	-	"	"	"	"
4/1W	1-6	0	"	I_{2N}-52 dB	-	"	I_N-38 dB	D_{4N}-29 dB	"
4/1X	1-7	0	"	"	-	"	"	"	"
4/1Y	1-8	50	"	"	-	"	"	"	"
4/1Z	1-9	200	"	"	-	"	"	"	"
4/1AA	1-10	0	"	D_{1N}-44 dB	-	"	"	"	

SHOT NO.	TRK-FILE	ADDED L(H)	OUTPUT	CH 1	CH 2	CH 3	CH 4	CH 5	COMMENTS
MONITORED THE SAME SENSORS AS 4/1W-AA EXCEPT THE OUTPUT WAS HARD-WIRED									
4/1BB	1-11	0	HW-TAIL	I_{2N}-52 dB	-	I-TAIL	I_N-38 dB	D_{4N}-29 dB	CH1-NC
4/1CC	1-12	50	"	"	-	1000X	"	"	"
4/1DD	1-13	200	"	"	-	"	"	"	"
MONITORED THE FUSELAGE WIRES INDUCED VOLTAGE AND CURRENT AND B_{1N} FOR BOTH HARD-WIRED AND ARC TESTS WITH DIFFERENT INDUCTANCE VALUES IN THE INPUT AND OUTPUT									
4/1EE	1-14	0	"	I_{3N}-12 dB	-	"	B_{1N}-20 dB	FW-35 dB	
4/1FF	0-0	0	"	"	-	"	"	"	
4/1GG	0-1	50	"	"	-	"	"	"	FW-POOR GND
4/1HH	0-2	50	"	"	-	"	"	"	"
4/1II	0-3	0	"	"	-	"	"	"	
4/1JJ	0-4	50	"	"	-	"	"	"	
4/1KK	0-5	200	"	"	-	"	"	"	
4/1LL	0-6	NOSE-200; TAIL-100	"	"	-	"	"	"	FW-POOR GND
4/1MM	0-7	NOSE-0, TAIL-100	"	"	-	"	"	"	
4/1NN	0-8	NOSE-0, TAIL-100	"	"	-	"	"	"	
4/1OO	0-9	NOSE-50; TAIL-100	"	"	-	"	"	"	
4/1PP	0-10	NOSE-200; TAIL-100	"	"	-	"	"	"	
4/1QQ	0-11	0	4" ARC-TAIL	"	-	"	"	"	
4/1RR	0-12	50	"	"	-	"	"	"	
4/1SS	0-13	50	8" ARC-TAIL	"	-	"	"	"	
4/1TT	0-14	0	"	"	-	"	"	"	
4/1UU	1-0	0	12" ARC-TAIL	"	-	"	"	"	
4/1VV	1-1	50	"	"	-	"	"	"	
4/1WW	1-2	50	14" ARC-TAIL	"	-	"	"	"	
4/1XX	1-3	50	13" ARC-TAIL	"	-	"	"	"	
4/1YY	1-4	0	"	"	-	"	"	"	
4/1ZZ	1-5	NOSE-0; TAIL-100	6" ARC-TAIL	"	-	"	"	"	
4/1AAA	1-6	"	"	"	-	"	"	"	
4/1BBB	1-7	NOSE-50; TAIL-100	"	"	-	"	"	"	
4/1CCC	1-8	NOSE-200; TAIL-100	"	"	-	"	"	"	

REFERENCES

[1] F. L. Pitts and T. F. Trost, "Analysis of Electromagnetic Fields on an F-106B Aircraft During Lightning Strikes," International Aerospace Conference on Lightning and Static Electricity, Oxford, England (March 1982).

[2] T. F. Trost and K. P. Zaepfel, "Broadband Electromagnetic Sensors for Aircraft Lightning Research," NASA Conference Publication 2128, FAA-RD-80-30 (22-24 April 1980).

[3] J. A. Plumer, "Lightning Safety Tests on NASA F-106B Thunderstorm Research Aircraft," LT-81-86 (26 April 1981).

1 Report No	2 Government Accession No	3 Recipient's Catalog No
NASA CR-166057		

4 Title and Subtitle	5 Report Date
NASA F-106B Lightning Tests	January 1983
	6 Performing Organization Code

7 Author(s)	8 Performing Organization Report No
Billy D. Heady and Keith S. Zeisel	MDC A7673
	10 Work Unit No

9 Performing Organization Name and Address	11 Contract or Grant No
McDonnell Douglas Corporation McDonnell Aircraft Company Box 516 St. Louis, Missouri 63166	NAS1-16202
	13 Type of Report and Period Covered
12 Sponsoring Agency Name and Address	Contractor Report
National Aeronautics and Space Administration Washington, DC 20546	14 Sponsoring Agency Code 505-34-43-50

15 Supplementary Notes

Langley Technical Monitor: Mitchel E. Thomas
Final Report

16 Abstract

This report summarizes a week of lightning simulation ground tests conducted on the NASA F-106B research aircraft prior to its 1982 flight program to elicit natural strikes. The purpose of the test program was to measure the response of the aircraft's electromagnetic sensors and interior wire circuits to a controlled ground test environment that simulates the electromagnetic effects of a lightning strike. Both direct attachment and radiated field tests were conducted. In most cases, the aircraft's engine was running and test data were gathered simultaneously from NASA and MCAIR sensors on both the aircraft's own instrumentation system and the remote MCAIR computer-controlled data acquisition system. During the direct attachment tests, the input inductance, output condition (hard-wired or spark gap), and the output location were varied to provide a wide variety of test conditions. The radiated tests to the isolated aircraft were conducted to excite and measure the natural resonances of the F-106B aircraft.

17 Key Words (Suggested by Author(s))	18 Distribution Statement
Lightning, lightning simulation ground test, electromagnetic effects of lightning strike, radiated fields, F-106 aircraft	UNCLASSIFIED - UNLIMITED Subject Category 47

19 Security Classif (of this report)	20 Security Classif (of this page)	21 No of Pages	22 Price
UNCLASSIFIED	UNCLASSIFIED	82	A05

For sale by the National Technical Information Service, Springfield Virginia 22161

End of Document